JASs Journal of Anthropological Sciences
Open Access
Research articles Vol. 103 (2025), pp. 73 - 112
doi. 10.4436/jass10307

Geometric morphometric data in cladistics: comparison with phylogenies inferred from morphological data

Margaux Simon-Maciejewski[1,2] , Giorgio Manzi[2,3], Valéry Zeitoun[4] & Aurélien Mounier[1,5,6]

1) Histoire Naturelle, PaléoFED, (HNHP, UMR 7194) CNRS/MNHN/UPVD, Musée de l'Homme, Paris, France
e-mail: margauxyveline.simonmaciejewski@gmail.com

2) Dipartimento di Biologia Ambientale, Sapienza Università di Roma, Rome, Italy

3) Istituto Italiano di Paleontologia Umana, Anagni (FR), Italy

4) UMR 7207-CR2P-CNRS-MNHN-Sorbonne Université, Campus Jussieu, Paris, France

5) Turkana Basin Institute, Nairobi, Kenya

6) CNRS, UAR 3129 – UMIFRE 11 3 Maison Française d'Oxford, Oxford, United Kingdom

Summary - *The development of protocols integrating 3D geometric morphometric data into cladistic analyses offers powerful tools to reassess previously established phylogenies. We examine evolutionary relationships within the genus* Homo *by comparing results from recently developed cladistic protocols using 3D data with an approach based on morphological characters. We applied both to 78 hominid calvaria - comprising 9 great apes, 45* Homo sapiens*, and 24 fossil specimens (2 australopithecines and 22 Homo) - grouped into 23 operational taxonomic units. The sample is described using 347 landmarks and 59 discrete characters, from which three datasets were generated. The first uses Procrustes-aligned 3D landmark coordinates. The second uses principal component coordinates from a Principal Component Analysis run on the aligned landmarks. The third dataset includes coded morphological features. Phylogenetic trees were constructed using TNT software following a three-step protocol. Firstly, a phylogenetic search using the heuristic algorithm under equal weight was performed. Secondly, the consistency and rescaled consistency indices for each character were extracted. Finally, a second phylogenetic search using the heuristic algorithm after reweighting of the characters was performed. The cladistic analyses of 3D data and discrete morphological traits yield different yet mostly congruent results, highlighting the strengths and limitations of each approach, and bringing new insight on long standing discussions in palaeoanthropology.*

Keywords - *Phylogeny, Geometric Morphometrics, Cladistics, Genus Homo, TNT software.*

Introduction

Geometric Morphometrics (GMM) is a set of methods developed to quantitatively assess changes in biological shape within a statistical framework (Rohlf and Bookstein 1987). These techniques have made significant contributions to various biological fields, such as morpho-functional studies, comparative anatomy, and evolutionary biology (Zelditch et al. 2004). In GMM, shape refers to the geometric information of an object after removing the effects of size and rotation, often through the use of General Procrustes Analysis (GPA), which aligns multiple datasets by minimizing non-shape-related differences (Kendall 1977). This allows for the examination of shape as an independent entity, which is essential for comparing organisms based on their form. The use of landmarks, or anatomical points that can be consistently identified across specimens, is central to this approach, providing a stable reference for shape analysis (Bookstein 1991).

When GMM is applied in the context of cladistics, the methods aim to explain the evolutionary relationships among species based on shared shapes (Bookstein 1991). Cladistics involves

selecting the phylogenetic tree that best explains the observed similarities through common ancestry. This favours the most parsimonious explanation—one that minimizes the number of evolutionary changes. This principle is known as parsimony (Nelson 1978). However, not all similarities between species can be explained by common ancestry, and those that cannot are termed homoplasies (Felsenstein 2004). The challenge in combining GMM with cladistics arises in how to interpret and quantify continuous variation in landmark data. This can lead to ambiguities in the phylogenetic tree. Ambiguity arises when multiple optimal states are possible for certain nodes, and continuous characters are often represented as ranges of possible values (Goloboff et al. 2006; Thiele 1993).

In this context, parsimony plays a critical role in determining the most parsimonious state reconstructions for continuous characters. However, as continuous variation is often difficult to discretize, the problem of deciding where to "draw the line" between character states becomes a key issue (MacLeod et al. 2002; O'Hara 1988; Thiele 1993). For example, the presence of continuous variation in traditional morphological characters—such as body size or shape—can render difficult the classification of these traits into discrete states (Pleijel 1995).

The multidimensional nature of landmark data limits the application of cladistic methods, which are traditionally designed for discrete characters (Klingenberg and Monteiro 2005; Monteiro 2000; Rohlf 1998). Critics have pointed out that the binary nature of homology—where a character is either homologous or not—may not be suitable for shapes, as Bookstein (1994) notes, "any order is arbitrary" when dealing with shapes. This is because the geometric relationships between landmarks can vary depending on the reference systems and criteria used to assess them (Klingenberg 2010).

While GMM and cladistics each offer powerful tools for understanding biological variation and evolutionary relationships, their combination faces significant challenges. These challenges include the difficulty of incorporating continuous variation into cladistic analyses, the ambiguity in defining and ordering character states, and the need for more effective methods of landmark alignment (Rohlf 2001). Ultimately, the success of combining these methods depends on finding ways to reconcile the continuous nature of shape variation with the discrete nature of cladistic character states. Although protocols have been developed to address these challenges (González-José et al. 2008; MacLeod et al. 2002), they have faced significant criticism (Adams et al. 2011; O'Hara 1988) and have largely been abandoned in many fields.

With the development of numerous algorithms, it is now technically possible to apply a standardized protocol and achieve reliable results (e.g., Catalano et al. 2010; Lockwood et al. 2004; Parins-Fukuchi 2018; Rohlf 2002; Smith and Hendricks 2013). The primary focus of ongoing debates lies in the underlying theory, but as Zelditch (2004) highlighted, further experimentation is needed to address these issues and reach a consensus. In this context, we aim at empirically testing a protocol that integrates 3D data - landmark coordinates - and principal component (PC) coordinates and compare the outcomes with the analysis of traditional morphological characters. The protocol, derived from Mounier and Caparros (2015), comprises three main steps: first, performing an initial heuristic analysis with equal weight; second, extracting consistency and rescaled-consistency indices (i.e., CI and RC) to weight each character, and finally, conducting a second heuristic analysis to assess the impact of the weighted characters. By integrating these various data types and methodologies, we aim at advancing the integration of GMM and cladistics, ultimately improving the robustness of phylogenetic analyses in human evolution.

Materials and methods

Choice of operational taxonomic units (i.e., OTUs)

To conduct and evaluate phylogenetic reconstructions, we examined a variety of taxa within the Hominidae family Gray, 1825 (Tab. 1). The

outgroup taxa consist of three specimens each from the genera *Pongo*, *Gorilla*, and *Pan*. Female specimens were chosen to minimize potential biases related to pronounced secondary sexual traits, such as the sagittal crest, which are typically more prominent in male apes. The remaining 20 OTUs included representatives from the genera *Homo* and *Australopithecus* (see Table 1 and Supplementary Material 1).

The study includes 78 specimens in total (see, Table 1 and Supplementary Material 1). Cladistic analysis was performed at the population/species level, with shape data averaged for each population/species (see, "Modality of data processing" in Simon-Maciejewski et al. 2024), leading to the inclusion of 23 OTUs in the analysis.

Nature of the data

The 3D models were generated by one of the authors (AM) through three different approaches, chosen according to the available equipment and specimens: 1) medical computed tomography (CT) scans processed with Amira (v5.5, FEI); 2) photogrammetric techniques using Metashape software (v1.8.1) (PH), and 3) 3D surface scanning (OP) with an HDI Advance optical scanner (45µ accuracy, LMI), with subsequent processing in Flexscan (v3.3, LMI) (Supplementary Material 1).

The shape of the calvarium, i.e. the cranium without the facial and mandibular parts, was described by both landmarks and semi-landmarks with the latter allowed to slide (Bookstein 1997). The sliding procedures used in the present analyses, follows the method outlined in Gunz et al. (2005) and Gunz and Mitteroecker (2013) and has been applied in several prior studies (e.g., Mounier et al. 2020, 2024; Mounier and Mirazón Lahr 2019, 2016). The criterion used was bending energy, and the semi-landmarks were equally spaced across six patches: two on the frontal bone, two on the parietal bone, and two on the occipital bone, covering both the left and right sides. In total, 27 landmarks and 320 semi-landmarks were applied (Fig. 1 and Simon-Maciejewski et al. 2024), and data were gathered using Landmark software (IDAV, Wiley 2005).

Analyses were conducted separately on three different matrices, following the protocol of Mounier et al. (2016): matrix A (see Supplementary Material 2) includes the aligned 3D coordinates of landmarks and semi-landmarks (post-Generalized Procrustes analysis, GPA) representing the averaged morphology of the calvarium of each OTU. Matrix B (see Supplementary Material 3) consists of principal components (PCs) coordinates derived from a principal component analysis (PCA) (Abdi and Williams 2010) conducted on the aligned 3D landmarks and semi-landmarks of each OTU. Matrix C (see, Supplementary Material 4) contains 59 morphological characters describing the morphology of the calvarium (see, *Choice and observation of morphological characters* in Material and Methods), coded as discrete states ranging from 1 to 3 (Appendix).

Since bilateral landmarks tend to be largely symmetrical, the use of the whole calvarium could result in the lateral (semi-)landmarks being weighted twice as much as those located along the sagittal plane (see Palci and Lee 2019). To evaluate the impact of this imbalance, a second dataset was created by symmetrizing the configurations using GPA. In this version, landmarks and semi-landmarks on the left side were excluded (see Supplementary Material 5) after alignment, resulting in a 192 landmarks coordinates dataset.

Choice and observation of the morphological characters

59 morphological features were chosen to describe the morphology of the calvarium (Figure 2, Supplementary Material 4 and 6) from past studies (Barriel 1994; Mounier 2009; Mounier and Caparros 2015; Zeitoun 2003, 2000), where detailed descriptions of each character can be found (not included here due to space limitations). The definition of the states for the morphological feature is mostly based from Mounier and Caparros (2015) and Mounier et al. (2016), and the 59 morphological traits were observed on 3D models of the 78 specimens included in the study by one of us (MS) before being confronted to previous published studies (Barriel 1994; Mounier 2009; Zeitoun 2003, 2000).

***Tab. 1** - Summary of the 78 specimens used in the study, with their chronology and references, the site they were found and the scanning technique used.*

NAME OF THE OTU	SPECIMENS	CHRONOLOGY	SITE	SCANNING TECHNIQUE*	CHRONOLOGY'S REFERENCES
Gorilla	Gorilla 5, 11, 12	19-20th century	-	OP	-
Pongo	Pongo 2, 3, 6	19-20th century	-	OP	-
Pan	Pan 1, 6, 10	19-20th century	-	OP	-
A. africanus	STS5	2.07 Ma	Sterkfontein, South Africa	CT	(Broom and Robinson 1950; Schwarcz et al. 1994)
	STS71	2.61 -2.07 Ma	Sterkfontein, South Africa	CT	(Broom and Robinson 1950; Schwarcz et al. 1994)
Koobi Fora – *H. habilis s.l.*	KNM-ER 1470	~1.88 Ma	Koobi Fora, Kenya	PH	(Feibel et al. 1989
	KNM-ER 1813	~1.88 Ma	Koobi Fora, Kenya	PH	(Feibel et al. 1989)
Dmanisi	D2282	~1.77 Ma	Dmanisi, Georgia	PH	(Gabounia et al. 2000)
	D2700	~1.77 Ma	Dmanisi, Georgia	PH	(Gabounia et al. 2000)
Ngandong	Ngandong 7	108 - 117 ka	Ngandong, Solo River, Java, Indonesia	PH	(Rizal et al. 2020)
	Ngandong 14	108 - 117 ka	Ngandong, Solo River, Java, Indonesia	PH	(Rizal et al. 2020)
Sangiran	Sangiran 17	1.02 - 1.50 Ma	Sangiran, Java, Indonesia	PH	(Antón 2003; Antón and Swisher 2004; Larick et al. 2001)
	Sangiran 2	1.02 - 1.50 Ma	Sangiran, Java, Indonesia	CT	(Antón 2003; Antón and Swisher 2004; Larick et al. 2001)
Zhoukoudian	Sinanthropus III	~0.68 - 0.78 Ma	Zhoukoudian, Beijing, China	PH	(Shen et al. 2009)
	Sinanthropus XI	~0.68 - 0.78 Ma	Zhoukoudian, Beijing, China	PH	(Shen et al. 2009)
Koobi Fora – *H. ergaster*	KNM-ER 3733	~1.6 Ma	Koobi Fora, Kenya	PH	(Feibel et al. 1989)
	KNM-ER 3883	~1.6 Ma	Koobi Fora, Kenya	PH	(Feibel et al. 1989
Early Neandertals	Saccopastore 1	130-250 ka	Saccopastore, Italy	PH	(Marra et al. 2015)
	Ehringsdorf H	~200 ka	Ehringsdorf, Germany	PH	(Grün and Stringer 1991)
Near East Neandertals	Amud 1	50-60 ka	Amud, Israel	OP	(Grün and Stringer 1991; Rink et al. 2001)
	Shanidar 1	60 - 80 ka	Shanidar, Irak	PH	(Trinkaus 1991)
Classic Neandertals	Monte Circeo 1	52 +/- 12 ka	Monte Circeo, Italy	CT	
	La Chapelle-aux-Saints	~50 ka	La-Chapelle-aux-Saints, France	CT	(Grün and Stringer 1991)
	La Ferrassie 1	53-66 ka	La Ferassie, France	CT	(Blackwell et al. 2007)

***Tab. 1** - Continued.*

NAME OF THE OTU	SPECIMENS	CHRONOLOGY	SITE	SCANNING TECHNIQUE*	CHRONOLOGY'S REFERENCES
Skhūl - Qafzeh	Qafzeh6	~100 ka	Qafzeh, Israël	PH	(Grün et al. 2005; Grün and Stringer 1991)
	Qafzeh9	~100 ka	Qafzeh, Israël	OP	(Grün et al. 2005; Grün and Stringer 1991)
	SkhūlV	100 - 135 ka	Mugharet-es-Skhūl, Israël	CT	(Grün et al. 2005)
KhoiSan	Kh-1738, Kh-1751, Kh-3731, Kh-3732, Kh-5051	19-20th century	Republic of South Africa	CT	(Mounier and Mirazón Lahr 2019)
Haya	AF.23.0.20, AF.23.0.23, AF.23.0.109, AF.23.0.110, AF.23.0.112	19-20th century	Tanzania	CT	(Mounier and Mirazón Lahr 2019)
Kongo	AfC-1730, AfC-1777, AfC-4974, AfC-9639, AfC-9642	19-20th century	Congo, Angola, Gabon	CT, PH	(Mounier and Mirazón Lahr 2019)
Mande	AfW-5419, AfW-6089, AfW-9539, AfW-9543, AfW-9544	19-20th century	Mali, Guinea	CT, PH	(Mounier and Mirazón Lahr 2019)
Berber	AfN-18458, AfN-18459, AfN-18460, AfN-18464, AfN-18465	19-20th century	Marocco	PH	(Mounier and Mirazón Lahr 2019)
Papu	MEL076, MEL084, MEL085, MEL104, MEL130	19-20th century	Papouasia, New-Guinea	PH, CT	(Mounier and Mirazón Lahr 2019)
France	Eu.24.00.1, Eu-1036, Eu-1042, Eu-1051, Eu-1065	19-20th century	France	CT	(Mounier and Mirazón Lahr 2019)
China	EAS-ORSA0427, EAS-ORSA0550, EAS-ORSA0669, EAS-ORSA0670, EAS-ORSA1858	19-20th century	China	CT	(Mounier and Mirazón Lahr 2019)
Inuit	99.1-102, 99.1-103, 99.1-161, 99.1-168, 99.1-196	19-20th century	Alaska	CT	(Copes 2012)

* CT = CT-scanner; OP = optical scanner; PH = photogrammetry

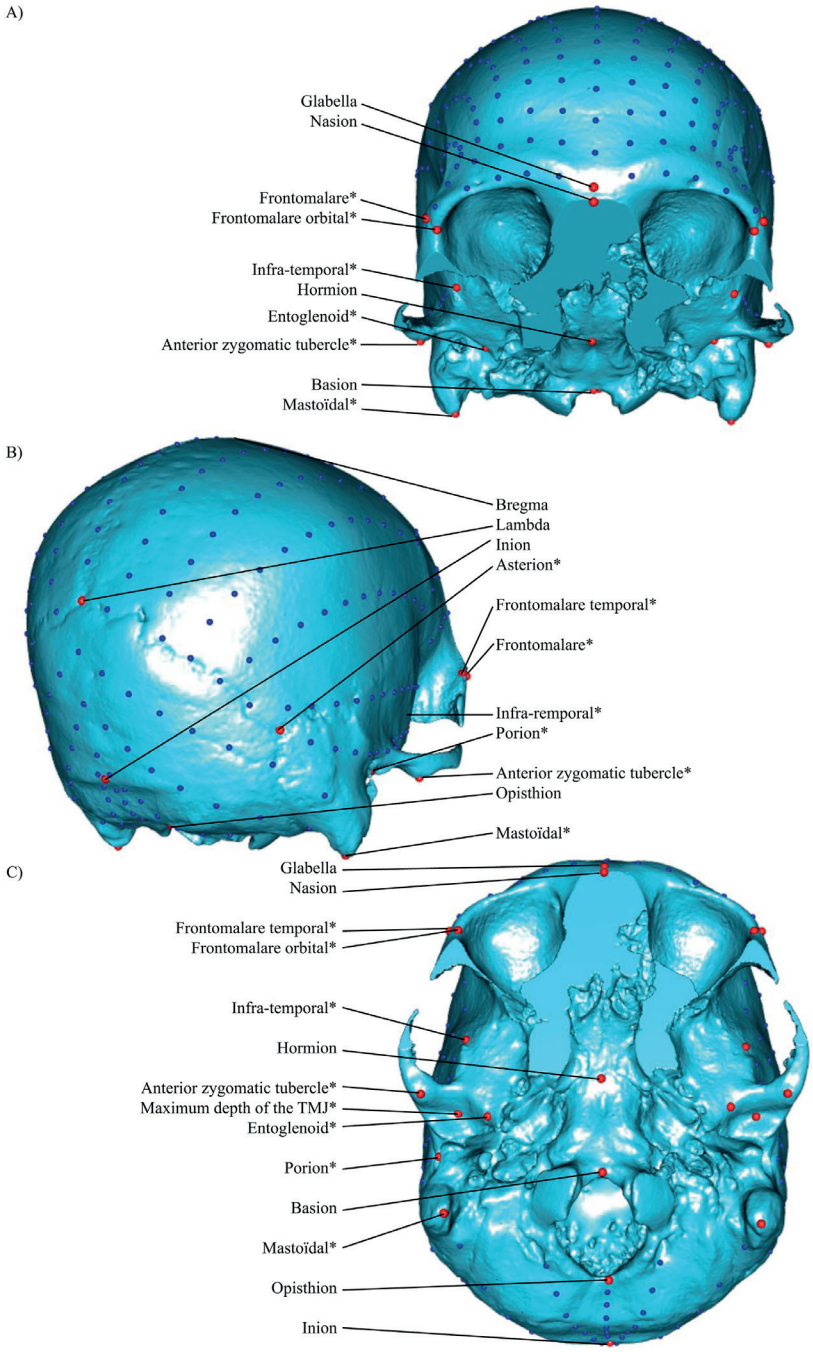

***Fig. 1** - Position of the 347 landmarks and semi-landmarks on the calvarium: A)* **norma facialis**, *B) ¾ posterior view, and C)* **norma basilaris**. *The landmarks with an asterisk "*" are bilateral.*

Phylogenetic analysis of the data

The TNT software from the Willi Hennig Society includes algorithms that allow the direct analysis of continuous (overlapping) quantitative data. These algorithms aim at reconstructing ancestral trait states by estimating shapes derived from landmarks, with the goal of parsimoniously minimizing the morphological evolution across the tree, using optimization logic (Catalano et al. 2010; Goloboff and Catalano 2011). This approach minimizes the displacement of individual landmarks between ancestors and descendants (Catalano et al. 2010; Goloboff and Catalano 2011; Simon-Maciejewski et al. 2024).

In each analysis, 20 OTUs from the genera *Homo* and *Australopithecus* formed the ingroup, while three OTUs representing the genera *Gorilla*, *Pan*, and *Pongo* were used as outgroups to root the search and polarize the transformations of the variables. The analyses were performed using TNT version 1.6 parsimony software (Goloboff and Morales 2023), which allows for the comparison of multiple relatedness hypotheses and the rapid identification of the most parsimonious tree. Parsimony was chosen because it allows the identification and discussion of the number and nature of synapomorphies observed at individual nodes (Matile et al. 1987).

In these analyses, characters were considered unordered, and no transformation cost matrix was used. The initial matrix analyses employed a heuristic algorithm with equal weighting (see Supplementary Material 7), random addition sequence (RAS), and tree bisection and reconnection (TBR) for branch swapping. This method divides the tree into subtrees, rearranges, and reconnects them until the trees with the shortest tree is determined.

Six parsimony phylogenetic analyses were conducted, corresponding to the analysis of the three different matrices, with the reweighting according to two indices: the consistency index (i.e. CI) and the rescaled consistency index (i.e. RC), following the successive approximative weighting method (SAW) of Farris (1969) (see, "Scripts"). Farris proposed a method to evaluate homoplasy using trees generated from an initial set of weights. He suggested using the levels of homoplasy observed to adjust the weights assigned to the characters and then conduct a new analysis with these updated weights. This iterative process continues until the new weights match those from the previous round (Farris 1969). However, as others, this weighting method is not without biases. Using the consistency index (CI) provides insights into the homoplasy associated with each character, i.e., a CI of 1 indicate the absence of homoplasy, while a CI of 0 represents a homoplastic character (Farris 1983, 1989), but it diminishes the influence of multistate characters. Consequently, for a similar number of steps, binary characters tend to have a greater impact than multistate characters (Goloboff 2022a,b). To address these issues, we opted to compare the CI with the rescaled consistency index (i.e., RC) (Farris 1989), which combines the CI and the retention index (RI). The RC will measure the proportion of maximum observable homoplasy and will achieve 0 when a character fits the tree as poorly as possible (Farris 1989; Goloboff 2022b). We chose not to use the RI to weight the character because the tree with the highest RI may not be the shortest, and it tends to assign greater "weight" to characters with less informative variation (Goloboff 2022b). Given these considerations, we chose the SAW method because it helps reduce bias from homoplasy by adjusting character weights. This ensures that less informative characters, which may contribute to homoplasy, are given less weight, while more informative characters are prioritized (Goloboff 2022b). Additionally, SAW offers flexibility in handling complex datasets, allowing for more accurate reflection of evolutionary relationships among OTUs. This leads to better tree resolution and reduces the effects of convergent evolution or reversals. In the present study, however, to avoid the risk of circularity, the SAW procedure was applied in a single iteration only, using the CI- or RC-derived weights from the first run without further reweighting cycles. Overall, SAW helps create a more reliable and balanced interpretation of the data, improving the robustness of the phylogenetic analysis (Farris 1969).

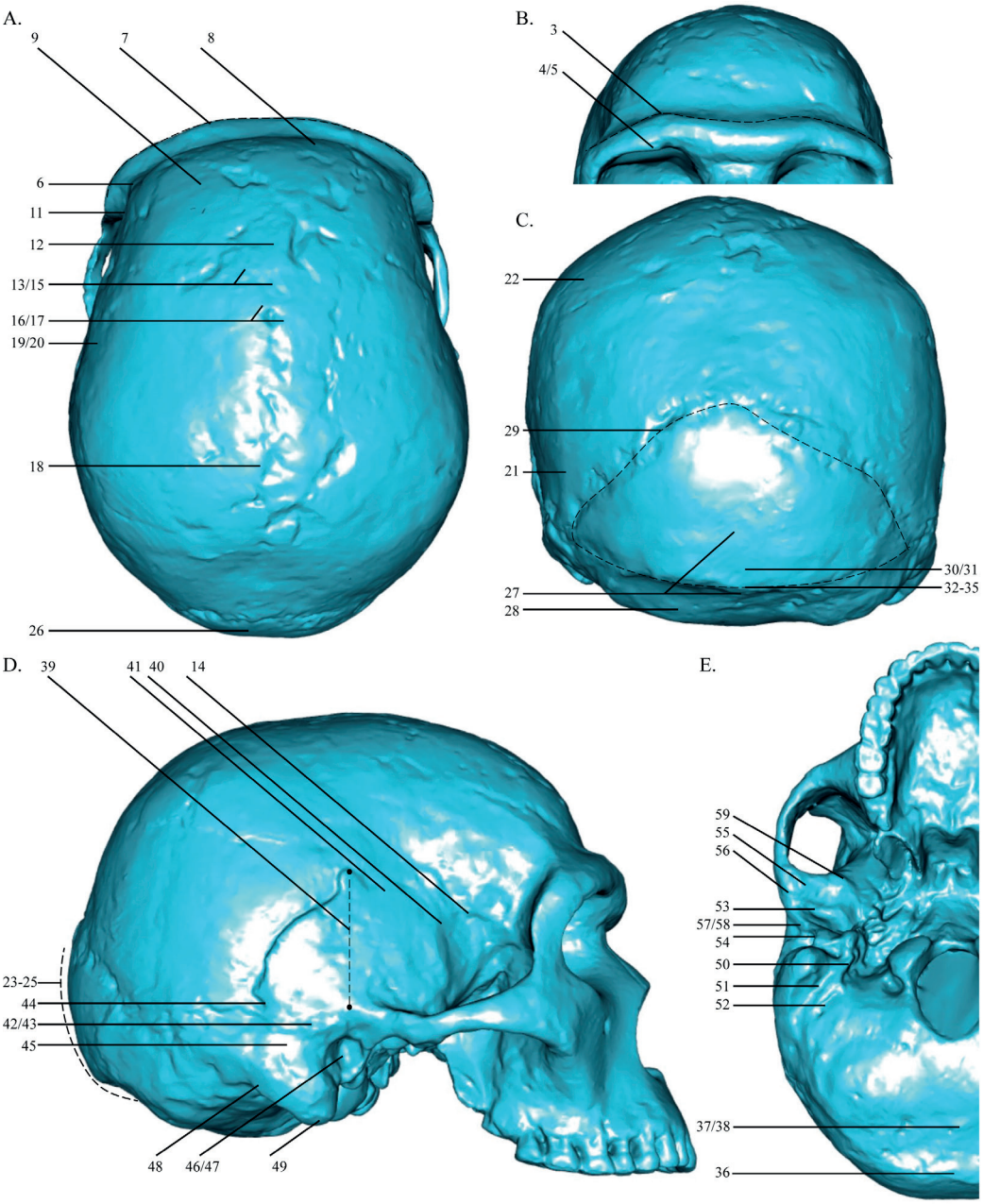

***Fig. 2** - Position of the morphological characters on the calvarium: **A.** norma verticalis **B.** norma facialis; **C.** norma occipitalis; **D.** norma lateralis, and **E.** norma basilaris.*

Although alternative weighting schemes—such as implied weighting (Goloboff 1993) or broader sensitivity analyses—were considered, they were not implemented here because they require additional assumptions about character fit, homoplasy distribution, and the expectation that characters vary in their reliability. In the present dataset, however, these assumptions are difficult to justify: the landmark-derived characters are numerous, mathematically interdependent, and not associated with discrete, biologically interpretable states, making it unclear how differences in fit should be meaningfully attributed to individual variables. Instead, the focus was placed on a controlled comparison of CI- and RC-based SAW weights.

After the reweighting process a subsequent tree search was run using the heuristic algorithm implemented in the software. The strict consensus was finally calculated.

To assess the robustness of the trees, the CI and RI were calculated. The CI was used to indicate the degree of homoplasy in each tree. However, if a tree has a high number of autapomorphies, this index may be artificially high (closer to 1), regardless of the homoplasy content of the other traits. To address this, we also calculated the RI of each tree, which represents the ratio between the maximum and observed number of homoplasies.

Evaluating the performance of a phylogenetic method can be challenging, as the "real" phylogeny cannot often be known. One of the approach used is based on a congruence criterion, commonly used in cladistic (Wheeler 2001). To assess the accuracy and reliability of the GMM data, the trees obtained from matrices A and B are compared to a reference phylogeny based on an independent source of evidence. In this study the reference topology is the tree obtained from the morphological matrix (i.e., Matrix C), as molecular data are not available for most of the specimens sampled. To minimize the effect of the weighting, we compared each topology with the one derived from the same weighting (for example, the tree from matrix C from CI-weighting versus the tree from matrix A from CI-weighting). The level of concordance was then measured by calculating the number of SPR (Subtree Pruning and Regrafting) moves (Goloboff 2007). This metric represents the inverse of the number of SPR moves needed to transform one tree into the other, divided by T-2, where T is the number of taxa (Goloboff 2007). We also calculated Robinson-Foulds distances (RF, Robinson and Foulds 1981) to further assess topological similarity. Higher SPR values and RF distances indicates greater dissimilarity, and therefore lower congruence, (i.e., a tree with a SPR value or RF distance of 0.4 will be more congruent than one with 0.6).

To assess the influence of allometry on shape, a linear regression of shape coordinates was performed on centroid size using "lm()" function (Chambers 1992) on R, and then the residuals were submitted to the same phylogenetic protocol described previously.

The robustness of each branch was finally assessed through 100 standard bootstrap replications (following Felsenstein 1985) and combined Bremer support (Goloboff 2014).

Scripts

In this study, the software TNT is used to run the analyses. It is an interactive program, that can read command from instructions files, allowing the automatization of protocols (Goloboff et al. 2008). In order to apply this protocol to the three matrices, we developed a script (see Supplementary Material 8) divided into five parts: first, extracting all necessary values (e.g., minimum and maximum steps); second, calculating the CI and RC of each character; third, weighting each character based on its CI and RC; four, comparing the length of the newly obtained tree to the length of the previous one. If the trees have the same length, the search stops, having found the most parsimonious tree. If they differ, the search continues until identical trees are obtained. And finally, the strict consensus of the most parsimonious trees is calculated.

Results

The two analyses (i.e., CI-weight and RC-weight) of matrices A, B and C (i.e., respectively composed of 347 landmarks, 22 PCs and

59 morphological characters) resulted, in each case, in several trees (see Figures 3 to 8). While the length and indices of each tree varies according to the weighting applied (see Table 2), the topologies of the trees do not change for matrix A when using the CI and RC weighting (see Table 4). For matrices B and C, polytomies are found in the *H. sapiens* populations, one at the root of the ingroup for matrix B and in the Neanderthals for matrix C (see Table 4).

With the CI-weighting, matrix A produces one parsimonious tree of 13.35 steps, with a CI of 0.831 and RI of 0.803 (Fig. 3, Tab. 2). The heuristic analysis of matrix B results in a 108.654 steps long phylogenetic tree with a CI of 0.486 and a RI of 0.698 (Fig. 5, Tab. 2). Heuristic analysis of matrix C results in one parsimonious tree that unresolves the relationships between the *H. sapiens* populations (Node M of Figure 7) and the relationships of the different Neanderthals OTUs (Node L of Figure 7). The tree is of 7497 steps with a CI of 0.636 and a RI of 0.829 (Fig, 7 and Tab. 2).

After weighting using the RC values, matrix A analysis generated one tree of 11.176 steps, with a CI of 0.831 and RI of 0.725 (Fig. 4, Tab. 2). The most parsimonious tree of matrix B is 49.963 steps long, with a CI of 0.686 and a RI of 0.887 (Fig. 6, Tab. 2). Heuristic analysis of matrix C results in a unique phylogenetic tree of 5327 steps with a CI of 0.709 and a RI of 0.883 (Fig. 8, Tab. 2).

The CI and RI indices of the parsimony trees derived from the analyses of the three matrices are relatively high, being overall superior to 0.5 - with matrix A yielding, overall, higher values - and reflect a robust phylogenetic signal (see, Table 2). We can observe that the length of the most parsimonious tree of each analysis is smaller with the RC weighting, rather than the CI weighting.

The results derived from the symmetrised half-calvarium dataset processed via GPA are congruent as well (see Supplementary Material 9). Using the landmarks-based matrix, the results are consistent, showing topologies similar to those obtained from the complete calvarium analysis (see Supplementary Material 9.1). The primary difference appears in the PC-matrix trees (see Supplementary Material 9.2): in two of the analyses (equal-weight and CI-weight), "Koobi Fora – *H. ergaster*" clusters with Neanderthals and *H. sapiens*, whereas in the RC-weight analysis, it is instead "Koobi Fora – *H. habilis* s. l." that groups with Neanderthals and *H. sapiens*. However, the indices are higher, and the numbers of steps are shorter.

Overall, the topology derived from PCs coordinates showed the highest congruence based on both SPR and RF metrics, with SPR values of 0.238 and 0.333 for CI-weighting and RC weighting respectively, and RF distance of 0.5 and 0.524. In contrast, Matrix A produced trees with SPR similarity values above 0.4 and RF distances above 0.55 when CI and RC weightings are applied, indicating significant incongruence. This indicates that the results of the PC coordinates are overall closer to the matrix C results than the 3D landmarks coordinate results.

The linear regression of shape (22 principal components) against centroid size revealed significant allometric effects restricted to the first three principal components (see Supplementary Material 10). The remaining components showed no detectable relationship with size. Following the removal of allometric signal by using the residuals from this regression in phylogenetic reconstruction, the resulting trees displayed low topological coherence and failed to recover expected evolutionary relationships (Supplementary Material 10). This suggests that the residualised shape data, while size-free, may lack sufficient phylogenetic signal for robust inference.

Matrix A of 347 landmarks coordinates. The most parsimonious trees, derived from the two-step analysis of matrix A, reveals several key patterns found in both trees (i.e., CI-weighting and RC-weighting) (Figs. 3 and 4). Node D, which supports the monophyly of the ingroup, is backed by a bootstrap value of 100% and a combined Bremer support of 100% (see Supplementary Material 11). There are observable changes that can be visualized through 3D

Tab. 2 - Length, consistency and retention indices of the tree for each analysis.

	WEIGHTING	LENGTH	CI VALUE	RI VALUE
MATRIX A - LANDMARKS COORDINATES	CI	13.3540022	0.831	0.803
	RC	11.175915	0.831	0.725
MATRIX B - PCS COORDINATES	CI	108.654	0.486	0.698
	RC	49.963	0.686	0.887
MATRIX C - MORPHOLOGICAL CHARACTERS	CI	7497	0.636	0.829
	RC	5327	0.709	0.883

Tab. 3- Topological correspondence (SPR moves and Robinson-Foulds distances) between the reference phylogeny and the trees derived from the three matrices. The average SPR similarity is 0.357 and the average RF distance is 0.541.

	WEIGHTING	SPR SIMILARITY	RF DISTANCE
MATRIX A - LANDMARKS COORDINATES	CI	0.428	0.571
	RC	0.428	0.571
MATRIX B - PCS COORDINATES	CI	0.238	0.5
	RC	0.333	0.524

shapes (see, Figures 3 and 4 and Supplementary Material 12). Overall, in *norma facialis*, the *sulcus supraorbitalis* in the supraorbital region is present, but the *arcus superciliaris* and *supraorbitalis* are not merged, and the postorbital constriction is less pronounced compared to that seen in apes. In *norma occipitalis*, we can observe the presence of an occipital bun and the appearance of the *processus retromastoideus*; we can also observe that the cranial outline, defined by the position of the greatest cranial width (bi-euryon), adopts a triangular ('tent-like') shape (Grimaud 1982). In *norma lateralis*, the profile of the antero-posterior frontal bone is more convex than in apes, and the transition between the *planum occipital* and *planum nucale* is rounded, in contrast to the angular transition seen in apes, with the opisthocranion positioned lower.

At node G, two clades are formed. The first, contains Dmanisi, Sangiran and Zhoukoudian (node H); while the second includes Ngandong, the Neanderthals and *H. sapiens* (node J). Morphological changes at node G includes, in *norma verticalis*, a supraorbital profile changing from medially concave at the glabella (node F) to straight; in *norma occipitalis*, the appearance of a *processus retromastoideus*, which then disappears (node J), and the presence of a triangular cranial outline, contrasting with the more, but not fully, circular shape observed at node J.

At node H, a clade is observed grouping Zhoukoudian, Sangiran, and Dmanisi, to the exclusion of Ngandong. This node is supported by a bootstrap value of 100% and a combined Bremer support of 100% (see Supplementary Material 11). Node I, which groups Sangiran and Dmanisi, is supported by a value of 8% for CI-weighting and 20% for RC-weighting and a combined Bremer support of 100% (see Supplementary Material 11). The changes in

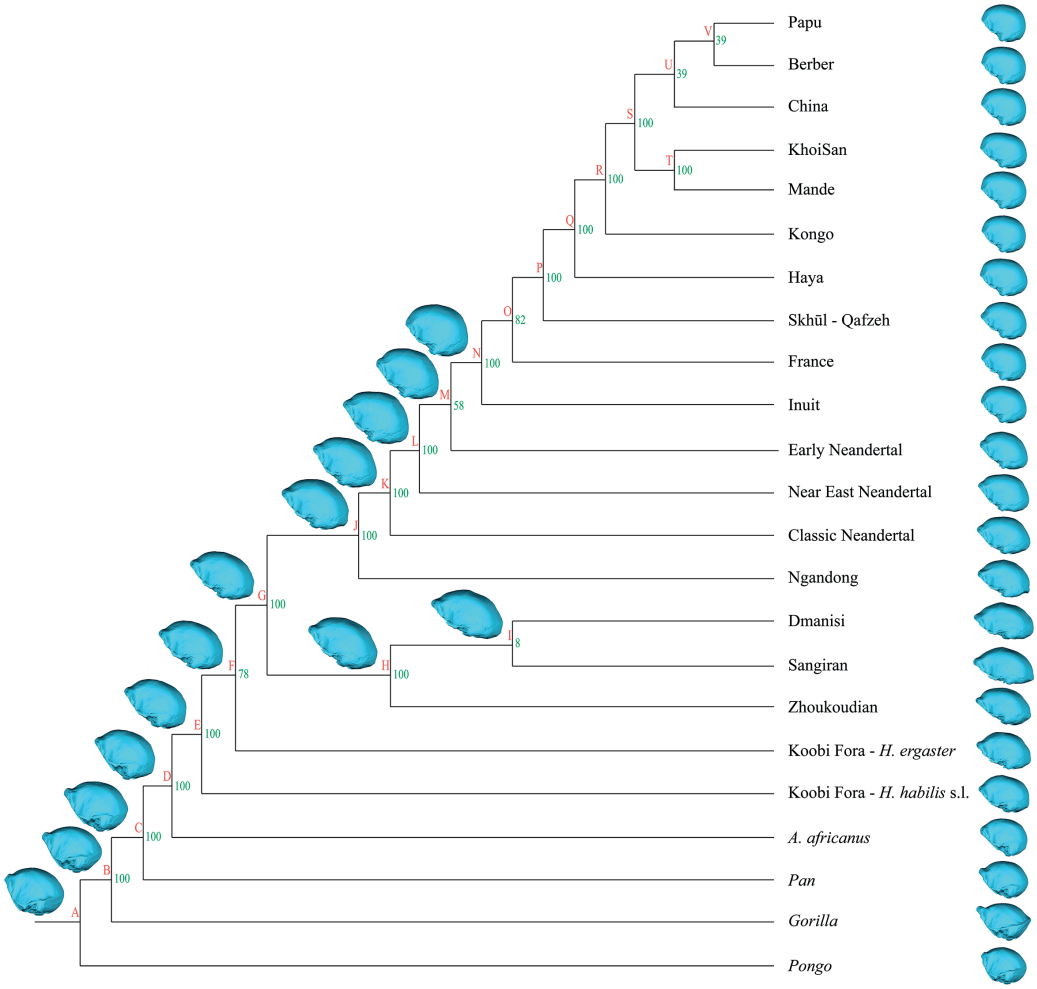

***Fig. 3** - Unique phylogenetic tree based on the analysis of matrix A after CI-weighting (i.e., 347 landmarks and 23 OTUs), 13.35 steps (CI = 0.831 and RI = 0.803). Values shown in green represent bootstrap scores in percentage (%) after 100 replications. Red letters are used to identify each node.*

the landmark's coordinates (see, Supplementary Material 12), which describe shape changes of the calvarium, at node H includes, in *norma verticalis*, the transition from a rectilinear supraorbital profile to a convex one, and in *norma lateralis*, the angle between the *planum occipital* and *planum nucale* become more pronounced compared to the other OTUs. In *norma occipitalis*, the *processus retromastoideus* and the *torus occipitalis transversus* are present, with the later, medially protruding, and the cranial outline is triangular ('tent-like') (Grimaud 1982), in contrast to the circular ('bomb-like') shape seen in Neanderthals (Boule 1913, 1912, 1911; Condemi 1992; Vandermeersch 1981).

In those trees, Neanderthals appear paraphyletic, while *H. sapiens* forms a monophyletic group at node N, supported by a bootstrap value of 100% and a combined Bremer support of 100% (see, Supplementary Material 11). The calvarium shape at this node exhibits the general characteristics of *H. sapiens* skull (see, Supplementary

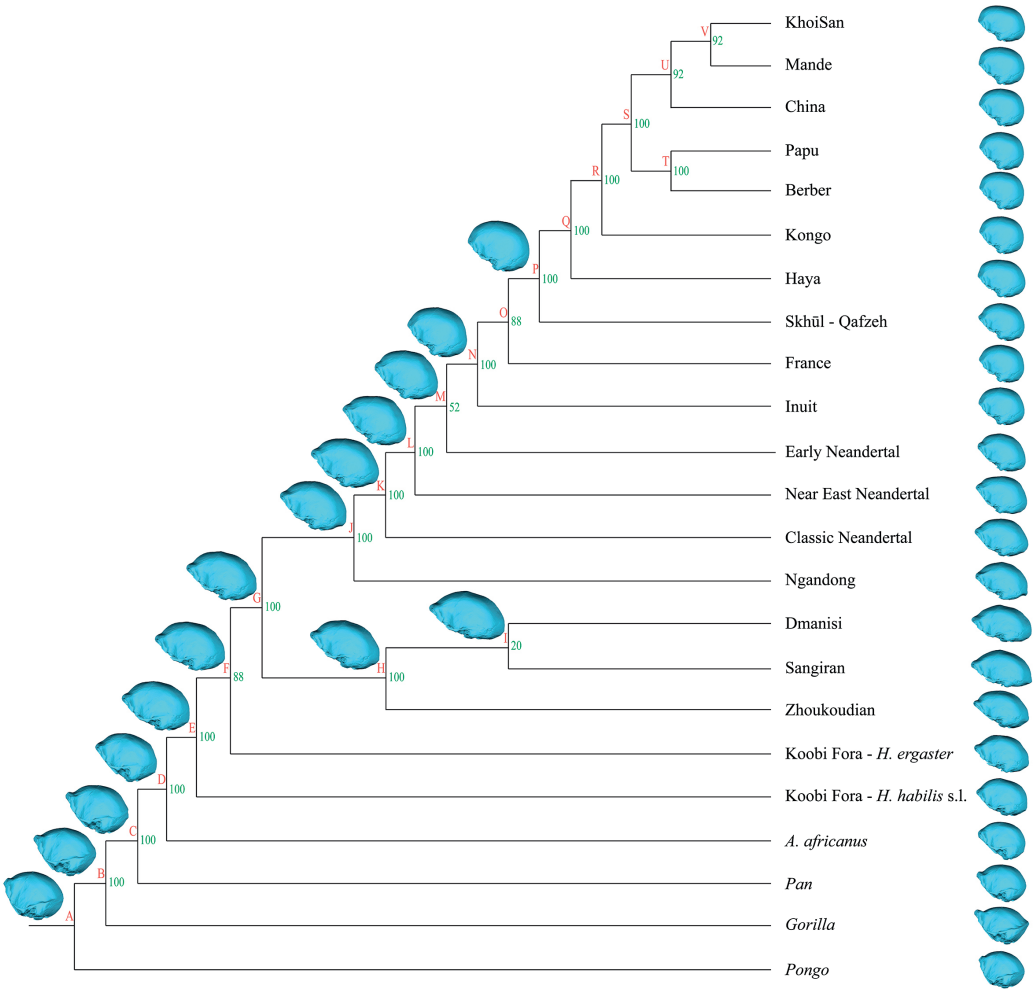

***Fig. 4** - Unique phylogenetic tree based on the analysis of matrix A after RC-weighting (i.e., 347 landmarks and 23 OTUs), 11.17 steps (CI = 0.831 and RI = 0.725). Values shown in green represent bootstrap scores in percentage (%) after 100 replications. Red letters are used to identify each node.*

Material 12), in *norma occipitalis*, the outline of the *planum occipitale* is pentagonal, the *torus occipitalis transversus* disappear, and the cranial outline presents a pentagonal shape ('house-like') (Broca 1868; Olivier 1960). In *norma verticalis*, the profile of the supraorbital region is convex. Finally, in *norma lateralis*, the convexity of the antero-posterior frontal bone is highly pronounced, and the angle between the *planum occipital* and *planum nucale* is entirely absent.

Matrix B of 22 PCs. The most parsimonious trees derived from the two-step analysis of matrix B reveals several key patterns found in both trees (Figs. 5 and 6).

Node D formation is explained by a shift from -0.107 to -0.05 in PC1. The morphological changes indicated by those values are, for the most, similar to those observed in the analysis of the matrix A (see Figures 5 and 6, and Supplementary Material 13): in *norma facialis*,

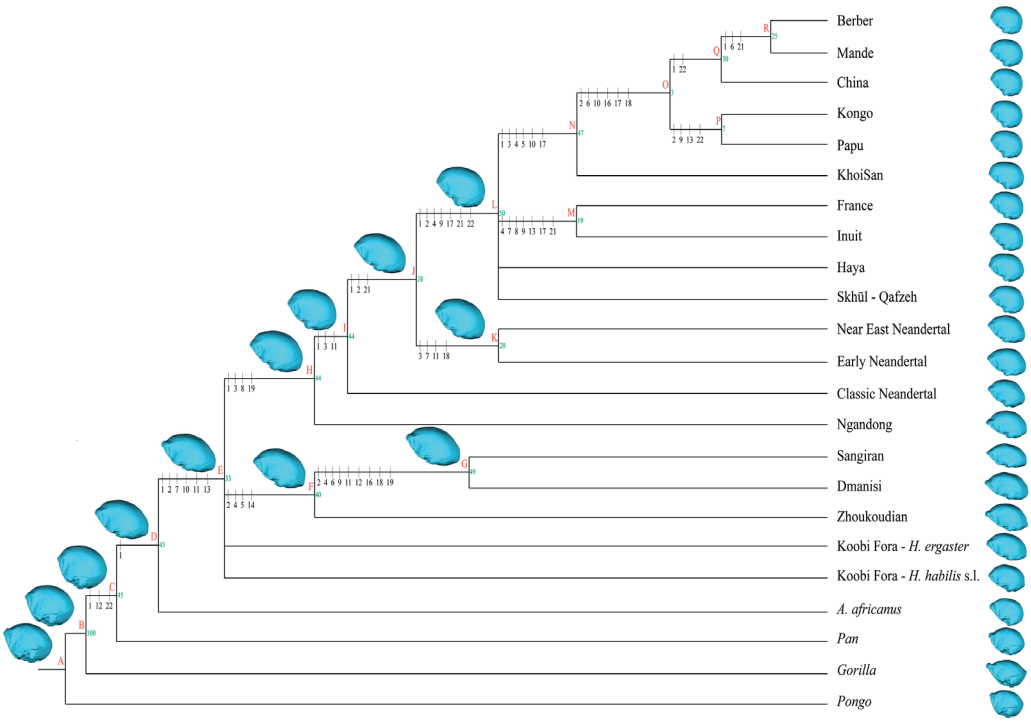

***Fig. 5** - Unique phylogenetic tree based on the analysis of matrix B after CI-weighting (i.e., 22 PC coordinates and 23 OTUs), 108.654 steps (CI = 0.486 and RI = 0.698). Values shown in green represent bootstrap scores in percentage (%) after 100 replications. Values shown under the branches are the number of the PC changing at each node. Red letters are used to identify each node.*

the *sulcus supraorbitalis* in the supraorbital region is present, but the *arcus superciliaris* and *supraorbitalis* are not merged, and the postorbital constriction is less pronounced compared to that seen in apes. In *norma lateralis*, the profile of the antero-posterior frontal bone is more convex than in apes and the transition between the *planum occipital* and *planum nucale* is rounded, with the opisthocranion positioned lower. In *norma occipitalis*, the occipital bun and the *processus retromastoideus* are also present, and the cranial outline is of triangular ('tent-like') shape (Grimaud 1982).

Node F supports a monophyletic group comprising Zhoukoudian, Sangiran, and Dmanisi, with the latter two forming a terminal clade at node G. those nodes are supported by bootstrap values of 40/64% and 49/76%, respectively, and a combined Bremer support of 100% (see Supplementary Material 11). The formation of node F is explained by shifts from -0,031 to -0,043 in PC2, from -0,01 to 0,02 in PC4, from -0,025 to -0,012 in PC5 and from -0,002 to -0,001 in PC14. The formation of node G is explained by shifts from -0,043 to -0,049 in PC2, from 0,002 to 0,007 in PC4, from 0.001 to -0.0055 in PC6, from -0.0066 to -0.005 in PC9, from 0.006 to 0.003 in PC11, from 0.0028 to 0.0017 in PC12, from -0.0007 to 0.0008 in PC16, from -0.00022 to -0.00016 in PC18 and from 0,00006 to 0,00096 in PC19. This changes in PC coordinates values refer to the same morphological changes as those described at nodes H and I from the analysis of matrix A (see Figures 5 and 6, and Supplementary Material 13). At node G, in *norma verticalis*, the supraorbital profile also goes from rectilinear in Zhoukoudian to concave in Sangiran and Dmanisi, and in *norma lateralis*, the angle between the *planum occipital*

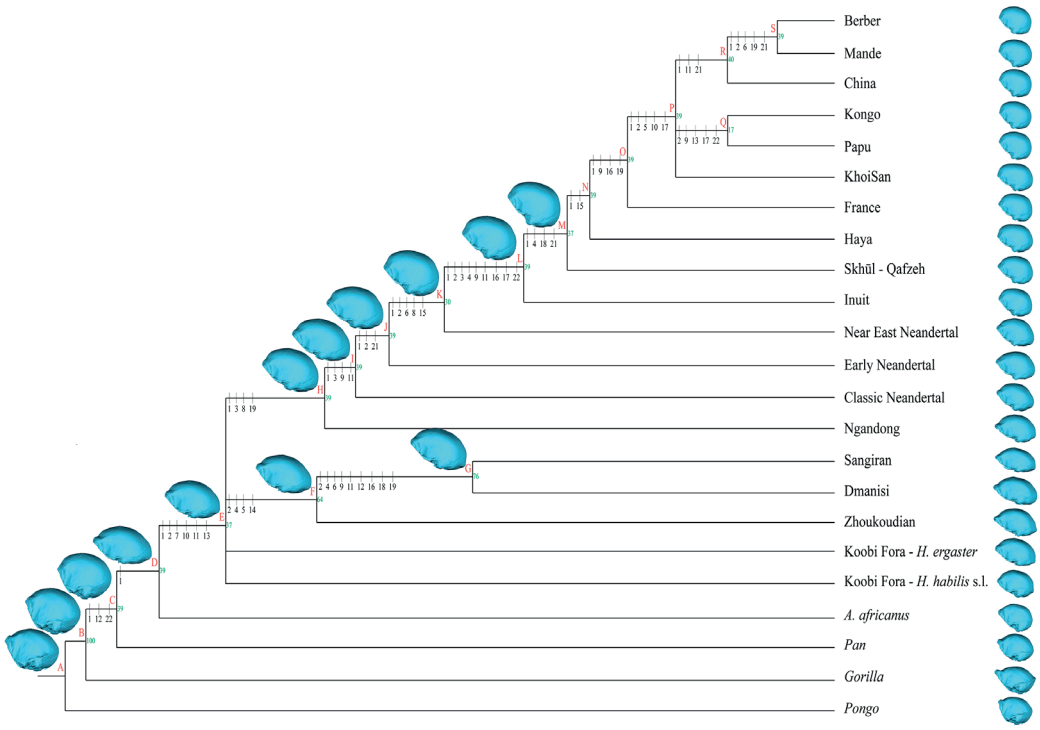

***Fig. 6** - Unique phylogenetic tree based on the analysis of matrix B after RC-weighting (i.e., 22 PC coordinates and 23 OTUs), 49.963 steps (CI = 0.686 and RI = 0.887). Values shown in green represent bootstrap scores in percentage (%) after 100 replications. Values shown under the branches are the number of the PC changing at each node. Red letters are used to identify each node.*

and *planum nucale* is more pronounced compared to the other OTUs. In *norma occipitalis*, the *torus occipitalis transversus* and the *processus retromastoideus* are present, and the cranial outline is triangular ('tent-like') (Grimaud 1982), in contrast to the circular ('bomb-like') shape seen in Neanderthals (Boule 1911, 1912, 1913; Condemi 1992; Vandermeersch 1981). Neanderthals are represented as a paraphyletic group from node I.

Node L, which includes the OTUs for *H. sapiens* (i.e., "Skhūl - Qafzeh" group and current populations), present bootstrap values of 50% (CI-weighting) and 39% (RC-weighting) and a combined Bremer support of 100% (see, Supplementary Material 11), and is supported by shifts from 0,018 to 0,05 in PC1, from -0,016 to 0,006 in PC2, from -0,033 to -0,0055 in PC3, from -0,0099 to -0,0054 in PC4, from 0,0039 to 0,0018 in PC9, from -0,002 to -0,0002 in PC11, from -0,0007 to -0,0012 PC16, from 0.0002 to 0.0039 in PC17 and from 0.00012 to 0.00046 in PC22. In terms of morphology, the changes observed at this node closely resemble those described following matrix A analysis (see, Figures 5 and 6 and Supplementary Material 13). In *norma facialis*, the *sulcus supraorbitalis* is present, with the *arcus superciliaris* and *arcus supraorbitalis* merged. In *norma occipitalis*, the outline of the *planum occipitale* and the cranial outline present a pentagonal shape, and the *torus occipitalis transversus* disappears. In *norma verticalis*, the profile of the supraorbital region is also convex, and in *norma lateralis*, the convexity of the antero-posterior frontal bone and the angulation between the *planum occipital* and *planum nucale* are identical to those previously observed with matrix A.

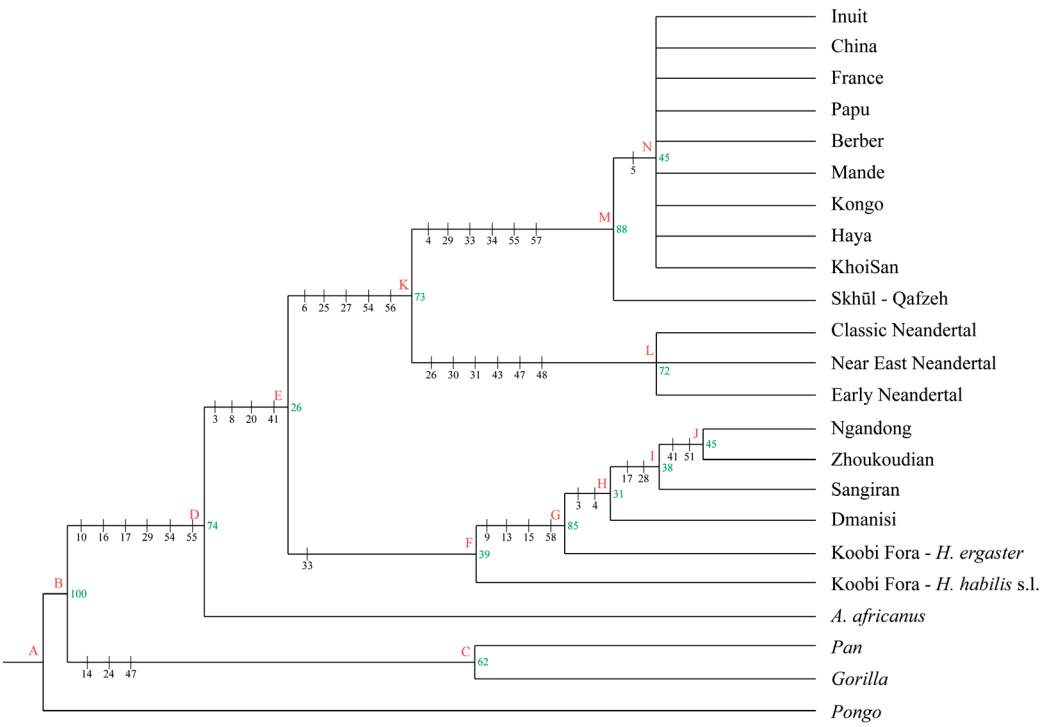

***Fig. 7** - Unique phylogenetic tree based on the analysis of matrix C after CI-weighting (i.e., 59 morphological characters and 23 OTUs), 7497 steps (CI = 0.636 and RI = 0.829). Values shown in green represent bootstrap scores in percentage (%) after 100 replications. Values shown under the branches, at each node, are the character number where a change in states occurred, showing synapomorphies. Red letters are used to identify each node.*

Matrix C of 59 morphological characters. The most parsimonious trees resulting from the two-step analysis of matrix C reveals a number of interesting trends found in both trees (Figs. 7 and 8). First, at node D, which is supported by a bootstrap value of 100% and a combined Bremer support of 100% (see Supplementary Material 11), the taxon *A. africanus* is separated from *H. habilis sensu lato*. Node F supports a monophyletic group consisting of "Koobi fora – *H. habilis* s.l.", "Koobi fora – *H. ergaster*" and the OTUs Dmanisi, Sangiran, Zhoukoudian and Ngandong, with the latter three taxa forming a terminal clade at node I. The formation of nodes F and I is supported by bootstrap values of 39% and 38% (CI-weighting) and by 42% and 43% (RC-weighting) and combined Bremer supports of 100% for each node (see Supplementary Material 11). The Neanderthals appear as a monophyletic group at node L, backed by a bootstrap of 72%/51%, respectively and a combined Bremer support of 100% (see Supplementary Material 11). At node M, which includes the OTUs representing *H. sapiens* ("Skhūl - Qafzeh" along with various *H. sapiens* populations), the formation of the node is supported by a bootstrap value of 88%/96%, respectively, and a combined Bremer support of 100% (see Supplementary Material 11).

Regarding the morphological changes supporting matrix C most parsimonious trees (Figs. 7 and 8; Supplementary Material and Supplementary Material 14), node D is explained by characters #10, 16, 17, 29, 54 and 55. They corresponds to several anatomical changes:, the antero-posterior convexity of the frontal (#10)

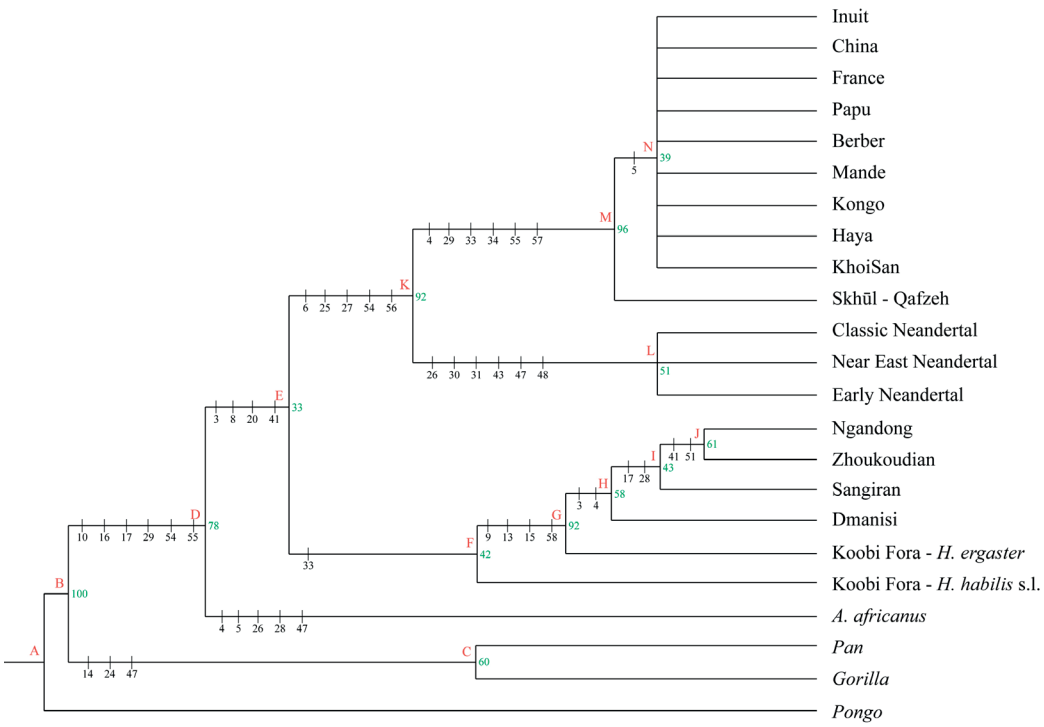

***Fig. 8** - Unique phylogenetic tree based on the analysis of matrix C after RC-weighting (i.e., 59 morphological characters and 23 OTUs), 5327 steps (CI = 0.709 and RI = 0.883). Values shown in green represent bootstrap scores in percentage (%) after 100 replications. Values shown under the branches, at each node, are the character number where a change in states occurred, showing synapomorphies. Red letters are used to identify each node.*

changes from weak (state 1) to intermediate (state 2); the sagittal keel on the bregma-lambda arch (#16) disappears (state 1), along with the parasagittal hollowing on both sides of the parietal suture (#17, state 1), the outline of the *planum occipitale* in *norma occipitalis* becomes circular (#29, state 2), the petro-tympanic crest is now orientated backward in relation to the sagittal plan (#54, state 3), and the articular tubercle presents a medio-lateral concavity (#55, state 1).

A. africanus is supported by five synapomorphies, which correspond to different states changes in characters #4, 5, 26, 28 and 47: the *sulcus supraorbitalis* in the supraorbital region (#4) goes from absent, with the *arcus superciliaris* and *supraorbitalis* merged (state 3), to complete (state 1), the projection of the supraorbital region (#5) is only observed on the *arcus superciliaris* (state 2); the occipital bun (#26) and the *processus retromastoideus* (#28) are now present (state 2), and finally the auditory meatus is in an intermediate position in relation to the *processus zygomaticus temporalis* (#47, state 2).

At node E, the clade is supported by a convex supraorbital region in *norma facialis* (#3, state 2), a continuous *sulcus postorbitalis* (#8, state 3), a low positioned *linea temporalis* on the parietal (#20, state 3), and curved or sinuous outline of the superior border of the temporal squama (#41, state 1).

Nodes F and I group together the Koobi Fora (i.e., *H. ergaster* and *H. habilis*) and Dmanisi specimens with fossils attributed to *H. erectus* (i.e., Ngandong, Zhoukoudian and Sangiran). The clades are supported respectively, by a medially protruding *torus occipitalis transversus* (#33, state 2)

***Tab. 4** - This summary table shows, for each matrix and weighting scheme, the node label subtending each taxon in the resulting phylogenetic trees. Letters indicate specific nodes, allowing direct comparison of whether a taxon is consistently associated with the same node across analyses. The layout highlights which clades remain stable and which show topological instability. For example, Gorilla appearing under node B in multiple trees indicates a stable clade. Some stable clades may receive different node labels across matrices (e.g., the Zhoukoudian–Sangiran–Dmanisi clade is node H in matrix A but node F in matrix B due to a polytomy).*

GROUP	MATRIX A		MATRIX B		MATRIX C	
	CI-WEIGHTING	RC-WEIGHTING	CI-WEIGHTING	RC-WEIGHTING	CI-WEIGHTING	RC-WEIGHTING
Pongo	A	A	A	A	A	A
Gorilla	B	B	B	B	B	B
Gorilla + *Pan*	/	/	/	/	C	C
Pan	C	C	C	C	/	/
A. africanus	D	D	D	D	D	D
Homo	/	/	/	/	E	E
Koobi Fora – *H habilis*	E	E	E	E	F	F
Koobi Fora – *H. ergaster*	F	F	/	/	G	G
H. erectus + Neandertals + *H. sapiens*	G	G	/	/	/	/
Dmanisi	/	/	/	/	H	H
Zhoukoudian	H	H	F	F	/	/
Sangiran	/	/	/	/	I	I
Sangiran + Dmanisi	I	I	G	G	/	/
Zhoukoudian + Ngandong	/	/	/	/	J	J
Ngandong	J	J	H	H	/	/
Neandertals + *H. sapiens*	/	/	J	/	K	K
H. neanderthalensis	/	/	/	/	L	L
Classic Neandertals	K	K	I	I	/	/
Near East Neandertals	L	L	/	K	/	/
Early Neandertals	M	L	/	J	/	/
Near East + Early Neandertals	/	/	K	/	/	/
H. sapiens	/	/	L	/	/	/
Skhūl - Qafzeh	P	P	/	M	M	M
Modern Humans	/	/	/	/	N	N

Tab. 4 - Continued.

GROUP	MATRIX A		MATRIX B		MATRIX C	
	CI-WEIGHTING	RC-WEIGHTING	CI-WEIGHTING	RC-WEIGHTING	CI-WEIGHTING	RC-WEIGHTING
Inuit	N	N	/	L	/	/
France	O	O	/	O	/	/
Inuit + France	/	/	M	/	/	/
Haya	Q	Q	L	L	/	/
Kongo	R	/	/	N	/	/
Kongo + Papu	/	/	/	Q	/	/
Berber + Mande	/	/	/	N	/	/
KhoiSan + Mande	T	V	/	/	/	/
China	U	U	/	R	/	/
Papu + Berber	V	T	/	/	/	/

and by the presence of parasagittal hollowing on both sides of the parietal sutures (#17, state 2) and of a *processus retromastoideus* (#28, state 2).

The Neanderthals appear as a monophyletic group from node L, supported by six synapomorphies: the occipital bun is present (#26, state 2), the suprainiac fossa is present (#30, state 3), with lateral edges that are converging upward (#31, state 2), the *crista supra mastoidea* is not aligned with the *processus zygomaticus temporalis* (#43, state 1), the auditory meatus is aligned with the *processus zygomaticus temporalis* (#47, state 3), and the *tuberculum mastoideum anterior* is present (#48, state 2).

Finally, node M, which groups all *H. sapiens* OTUs (including "Skhūl - Qafzeh" and various *H. sapiens* populations), is supported by six synapomorphies. This corresponds to the presence of a complete *sulcus supraorbitalis* in the supraorbital region (#4, state 1), to a pentagonal *planum occipitale* in *norma occipitalis* (#29, state 3), to the absence of a *torus occipitalis transversus* (#33 and 34, state 1); to an antero-posterior convexity of the articular tubercle (#55, state 2), and to a weakly-marked or absent *tuberculum zygomaticum posterius* (post glenoid process, #57, state 1).

Discussion

Geometric morphometric data in cladistics

The use of GMM data in cladistics has been subject to several criticisms, with two main issues often raised by researchers.

One of the primary concerns is the reliability of phylogenetic relationships inferred from morphometric characters, specifically whether landmark coordinates carry a phylogenetic signal, and the claim that cladistics using GMM data is no more informative than phenetic methods (Adams et al. 2011) with resultant phylogenies capturing only a phenetic signal. Researchers argue that "phylogenetic inference from morphometric data, or other high-dimensional phenotypic data in general, must be expected to be unreliable" (Varón-González et al. 2020). However, a number of studies have shown that some phylogenetic signal can be retrieved from morphometric characters (e.g., Catalano et al. 2015; Catalano and Torres 2017; Perrard et al. 2016). This is particularly relevant when the results obtained from morphometric data are congruent with established phylogenies. A study by Catalano and Torres (2017) further

emphasized that while overall performance of GMM data to infer phylogenies was modest, regardless of the method used, the inclusion of more anatomical structures tended to improve phylogenetic inferences and support the use of morphometric characters in cladistics. Moreover, with phenetic methods, such as neighbor-joining or UPGMA, the partitioning of shape variables is not crucial, as the analysis relies on distances between taxa. The result is not affected as long as relative positions in multidimensional space are used (Felsenstein 2004; Klingenberg and Gidaszewski 2010; Swofford et al. 1996), making trait definition less important. In contrast, cladistic approaches, especially those using Wagner parsimony, require characters to be discrete and independent—an assumption that clashes with the inherent interdependence of 3D landmark coordinates. Because parsimony treats each coordinate as an independent character, the strong covariance structure among Procrustes coordinates may artificially inflate character numbers and disproportionately influence tree searches. The present study acknowledges this issue, but further work is required to quantify its consequences—for instance, through targeted sensitivity tests assessing how dependence patterns affect tree length, support values, or recovered topologies. Nonetheless, landmark data still hold valuable phylogenetic information, particularly when integrated with other morphological traits that help contextualise shape variation (Goloboff 2022b). Recent work (Simon-Maciejewski et al. 2024) demonstrated that phylogenetic trees inferred from GMM data using cladistic methods were more robust and consistent with existing phylogenies than those generated by phenetic methods. Specifically, analyses using UPGMA and Neighbor-Joining on a PCA-derived coordinate matrix from a similar 347-landmarks dataset produced incongruent and unreliable trees, both with each other and with the established literature. These findings suggest that cladistic approaches applied to 3D GMM datasets may yield more stable and congruent results than phenetic ones. Wheeler (2021) also advocated for parsimony-based methods over distance-based ones, particularly for their ability to reconstruct ancestral states, reinforcing the methodological preference for cladistic over phenetic approaches in this context.

The second major point of contention concerns the dependence of characters. The question of trait definition and independence and how shape data should be conceptualized is central: as a single, unified trait or as a set of independent traits. The answer has implications for how these traits are then coded as characters or states in phylogenetic analyses (Bookstein 2002, 1991; MacLeod et al. 2002; Monteiro 2000; Rohlf 1998; Zelditch et al. 2004). However, it is important to note that this challenge is not exclusive to morphometric data. In fact, defining and assessing the independence of "traditional" discrete morphological characters presents similar difficulties, as their definitions can vary widely (e.g., Hawkins et al. 1997; Pleijel 1995; Pogue and Mickevich 1990; Sereno 2007; Thiele 1993) and their implications evaluated. We argue that the recognition of structures which are alternate forms is a vital stage of primary homology assessment and is equivalent to the conceptualization of a transformational homology. Such a view complies with the demand that characters are independent and that character states are hierarchically related. We identify one justifiable solution to the inapplicable data coding problem (coding for organisms which have red tails, blue tails or no tails, and their independence is often hard to establish (e.g., MacLeod et al. 2002; McCracken et al. 1999; Mounier et al. 2009). One possible advantage of morphometric data, however, is that PCs are mathematically independent. While PCs have their own limitations—such as interpretability—they offer a way to formally ensure character independence. In the results, PC-based representations even yielded slightly better phylogenetic results than raw landmark coordinates, suggesting that this approach may partly resolve the dependence issue. Nevertheless, the sensitivity of the PC-based topologies to weighting schemes indicates that this independence does not guarantee stability and must be interpreted with caution.

In this context, TNT software from the Willi Hennig Society stands out as the only major phylogenetic tool with algorithms specifically designed for continuous morphometric data. These algorithms reconstruct ancestral shapes directly from landmarks by minimizing morphological changes along phylogenetic trees (Catalano et al. 2010; Goloboff and Catalano 2011), offering a promising way for more nuanced phylogenetic inference using GMM data.

The present approach follows that of Catalano and Goloboff (2010) and Goloboff and Catalano (2011), phylogenetic morphometric, which operates on the coordinates of either the principal components or landmarks after alignment to minimize displacement between ancestors and descendants. This method estimates ancestral configurations at internal nodes in a similar way to traditional parsimony using discrete qualitative data but, in that case, each landmark coordinates are treated as a multivariate trait. The resulting ancestral patterns are composed of 3D landmark configuration which can be viewed through warping as fully rendered 3D morphologies. The ancestral position of a landmark is identified by exploring a grid of possible positions based on observed descendant landmarks, allowing for refinement through increased grid subdivisions or iterations around the initial estimation.

The primary goal of this study was to empirically test a protocol that integrates 3D data—landmark coordinates and principal component (PC) scores—and to compare the results with those obtained from the analysis of discrete morphological characters, assessing their congruence against a phylogeny derived from an independent source of information, in this case, morphological characters. To better understand the advantages and limitations of different data types in phylogenetic analysis, we examined the specific characteristics of each of the analysed matrices.

For matrix A, the analysis requires more time and more powerful computing resources. the nature of the data which is composed of aligned 3D coordinates allow for the reconstruction of 3D ancestral shapes at each node, providing a readily available visualisation of the morphological changes across the trees (see, Figures 3 and 4). Additionally, by using a large number of variables (i.e., 347 for A compared to 22 for B and 59 for C), it allows for a very detailed analysis of the morphological information of the OTUs. Using aligned landmark coordinates also has the advantage of resolving the discretization issues found in traditional morphological features, thereby reducing bias in state definitions and improving the quantification of shape differences. However, 3D landmark coordinates are mathematically interdependent and cannot be treated as independent variables. This raises important questions about character weighting and the possibility that covariance structures may exaggerate or obscure signal. Future work should incorporate formal sensitivity analyses, for example by selectively down-weighting blocks of correlated coordinates, permuting subsets of landmarks, or comparing results against randomized matrices to evaluate how dependence affects tree topology. One possible way to address this issue—though not explored in the present study—would be to analyse specific subsets of landmarks, such as those defining particular morphological traits or outlines. These subsets could be conceptually comparable to individual characters and might be treated as independent units of morphological information (see Catalano et al. 2015; Klingenberg 2010).

In contrast, matrix B employs dimensionality reduction through PCA, transforming original variables into independent, orthogonal variables (Jolliffe 2002). This approach addresses character dependency issues commonly associated with 3D geometric morphometric data. However, it has limitations when compared to matrix A. Like matrix A, it allows for ancestral shape reconstruction, but dimensionality reduction to just 22 features may distort the matrix. Results from an exploratory study showed that a smaller character set reduces the ability to account for the entire phylogenetic history between OTUs, hence limiting the ability to discern meaningful evolutionary relationships between taxa, while limiting homoplasy (Rohlf 2001). Another limitation is

that PCA scores represent a projection of the landmarks onto a single, unidimensional value. As a result, they do not reconstruct the ancestral shape but instead only indicate the point where the landmarks would have been projected. Moreover, this approach shifts the analysis from being shape-based to relying on one-dimensional variables, which do not inherently provide direct insights into actual shapes (Adams et al. 2011; Catalano et al. 2010; Goloboff 2022b; Monteiro 2000; Zelditch et al. 2004) and might not be meaningful, as the analyse of PCA scores from GM data rely on a phenetic analysis of overall similarity without regard to variation in individual morphological traits that represent hypotheses of primary homology (sensu de Pinna 1991) one related to comparisons among different organisms and the other restricted to comparisons within the same organism. The former is essentially hierarchical in nature, thus being in fact a less obvious form of taxic homology. The latter is logically equivalent to so-called serial homology in a broad sense (including homonomy, mass homology or iterative homology. The sensitivity of the PC-based trees to alternative weighting schemes in this study underscores these theoretical concerns and suggests that the apparent advantages of independence must be balanced against the potential loss of phylogenetically informative structure. However, our results indicate that they can still yield informative phylogenetic signal—suggesting that, despite theoretical limitations, the method may be practically effective in some contexts.

Matrix C, which uses 59 discrete morphological characters, describe less of the morphology of the calvarium but allows more straightforward discussions of synapomorphies at each node. While the characters in this matrix are morphologically separate, they are not necessarily independent, and their independence is rarely tested (e.g., McCracken et al. 1999). As with any definition of character and its various states (Pleijel 1995), challenges remain in character definition and states distinction, particularly with continuous variation, leading to potential loss of information when similar but not identical shapes are grouped in the same state. For instance, character 33, the *torus occipitalis transversus*, is categorized into three states: absent, present and medially protruding, and present and bilaterally protruding. In reality, the shape of this character is more nuanced and may vary between specimens included in the same OTU (Mounier 2009). These issues highlight that all three approaches—coordinates, PCs, and discrete characters—carry their own sources of bias, and comparisons between them must therefore be interpreted cautiously.

A further point concerns the strength of phylogenetic signal in the landmark coordinates themselves. As highlighted by recent critiques, establishing that morphometric data contain more hierarchical structure than expected by chance is essential for evaluating their suitability in cladistic inference. Although the present study did not implement formal tests of phylogenetic signal, several approaches could be adapted for future work—for example, comparing observed tree length distributions to those generated from randomized coordinate matrices, or applying extensions of classical signal metrics (e.g., Blomberg's K or Pagel's λ, Blomberg et al. 2003; Pagel 1999) to multivariate shape data. Such analyses would allow a clearer assessment of whether the covariation patterns captured by the landmarks meaningfully reflect phylogenetic structure rather than noise or spatial autocorrelation. Incorporating these tests will strengthen future evaluations of morphometric datasets in phylogenetic contexts.

The symmetrized analyses—based on landmark configurations restricted to a single half of the calvarium—are broadly consistent with the results obtained from the full-calvarium datasets, yet they display slightly greater topological instability, particularly in the PCA-derived trees. While the landmark-based matrices remain largely congruent with the complete-cranium analyses, the PC matrices show shifts in the position of the Koobi Fora specimens, which alternately cluster with *H. sapiens* and Neanderthals depending on the weighting scheme. This increased incongruence likely reflects the loss

of bilateral morphological information: by analysing only half of the calvarium, potentially informative asymmetries are excluded, reducing the phylogenetic signal. The differences observed here suggest that halving the configuration may remove structural correspondences that contribute to stability in the full dataset. Although the symmetrized half-calvarium approach remains useful—particularly for dealing with fragmentary fossils—its slightly reduced performance highlights the need to consider how much evolutionary information is embedded in bilateral or whole-vault patterns, and how their removal may influence tree topology, especially in PCA-based analyses. These results reinforce the broader conclusion that morphometric phylogenetic inference is highly sensitive to data treatment, landmark selection, and the handling of semi-landmarks, and should therefore be applied with caution (Cardini 2016; Klingenberg and McIntyre 1998).

Finally, although allometry was detected in the first three principal components, the phylogenetic trees generated from the size-corrected residuals yielded incoherent and biologically implausible topologies (see Supplementary Material 10). This outcome highlights a potential limitation of regressing out allometry in geometric morphometric analyses: while intended to isolate shape variation independent of size, the process may also remove evolutionarily meaningful signal, particularly when allometric trends are themselves phylogenetically structured (Giannini 2014; Klingenberg and Marugán-Lobón 2013; Pélabon et al. 2014). These results underscore the need for caution when applying allometry correction prior to phylogenetic inference, especially in datasets where size and shape covary in evolutionarily informative ways. More generally, the strong influence of allometry correction, symmetrisation, data filtering, and weighting demonstrates that conclusions drawn from morphometric phylogenetics remain provisional and should be interpreted with appropriate restraint until tested across larger samples, alternative sliding procedures, and complementary lines of evidence.

Palaeoanthropology

Overall, the main results of this study are aligned with generally accepted phylogenies. The positioning of the outgroups and the monophyly of *H. sapiens*, despite minor variations in the relationships among contemporary human populations, is found in all six analyses, showing a consistency in the results. The placement of the OTUs in the phylogenetic trees derived from the three matrices (A, B, and C) echoes historical taxonomic proposals on hominid evolution (Campbell 1963, 1962).

In one case, the phylogenetic relationships between "Koobi Fora – *H. habilis* s.l." and *A. africanus*, the six phylogenies resulting from the analysis of the different data matrix appears to yield to similar interpretations. In the trees obtained from matrices A and B, based on 347 landmark coordinates and 22 PCs coordinates, *A. africanus* (node D; see Figures 3 to 6) and "Koobi Fora – *habilis* s.l." (node E; see Figures 3 and 6) do not group together. These nodes are distinguished by several morphological differences: in *norma facialis*, the postorbital constriction is less pronounced in node E compared to node D, in *norma occipitalis*, an occipital bun is present in node D but absent in node E, and the cranial outline, marked by the position of the greatest cranial width (bieuryon), forms a more pronounced triangular shape in node D, whereas it is less defined in node E. In *norma lateralis*, the transition between the *planum occipital* and *planum nucale* is rounder in node E than in node D, with the opisthocranion positioned lower in node E. Similarly, the trees obtained from matrix C, which uses 59 traditional characters, separates the two taxa. It places *A. africanus* at the root of the genus *Homo* (node D), while grouping "Koobi Fora – *H. habilis* s.l." with *H. erectus* sensu lato at node F (see Figures 7 and 8). *A. africanus* is supported by five autapomorphies (see "Results"), whereas the grouping of the Koobi Fora specimens (referred to either *H. ergaster* or *H. habilis*) is supported by a single character, the presence of a medially protruding *torus occipitalis transversus*. In those trees, *A. africanus* and "Koobi Fora – *H. habilis* s.l." are separated by five features.

Thus, all the trees separate these OTUs based on the same morphological criteria, with a focus on the occipital bun, the outline of the supraorbital region, the *sulcus postorbitalis*, and the *torus occipitalis transversus*. Overall, the synapomorphies present in the trees obtained from matrix C are also observed in the trees obtained from matrices A and B, except when the character states are not as finely defined or when the shape does not exhibit the feature. For instance, the antero-posterior convexity of the frontal (character 10) is coded with three distinct states in the morphological matrix (i.e., C). In the resulting trees, *A. africanus* and "Koobi Fora – *H. habilis* s.l." share the same character state. However, in the trees obtained from matrices A and B, the shape differences are considered more explicitly and can be observed at nodes D and E. Additionally, the trees obtained from matrix C includes characters that are too subtle to be observed in the trees obtained from matrices A and B, such as the *linea temporalis* and the outline of the temporal squama.

The classification and interpretation of the hominins within *H. erectus* have long been a subject of debate. In the 1980s, researchers tended to classify *H. ergaster*, Sangiran, and Zhoukoudian as distinct species (Andrews 1984; Tattersall 1986; Wood 1984), while the defining features of *H. erectus* are generally found in both African and Asian specimens. Some researchers propose that *H. erectus* could be ancestral to *H. neanderthalensis* or that *H. erectus* and *H. sapiens* form a single highly variable group, with the Ngandong series sometimes referred to as *Homo soloensis* or *Homo sapiens soloensis* Dubois 1940 (Bonde 1989; Bräuer and Mbua 1992; Campbell 1963; Dubois 1940; Gingerich 1979; Jelinek 1981, 1980; Stringer 1987a; Tobias 1985; Von Koenigswald 1958; Widianto and Zeitoun 2003; Wolpoff 1980; Zeitoun et al. 2010). This view is supported by two of the trees (A and B, see Figures 3 to 6), which include the Ngandong series within a monophyletic group with Neanderthals and *H. sapiens*, excluding them from the clade comprising Dmanisi, Sangiran, and Zhoukoudian.

Regarding what is referred to as *H. erectus* sensu lato, the results show divergent outcomes in the different phylogenetic trees derived from the matrices. The trees obtained from matrix A shows that *H. erectus* sensu lato is paraphyletic; at node H, the Sangiran, Zhoukoudian, and Dmanisi form a monophyletic group, excluding Ngandong at node J and "Koobi fora – *H. ergaster*" at node F (see Figures 3 and 4); at node I, Sangiran and Dmanisi group together. Similarly, the trees obtained from matrix B shows identical groupings at node G and H (i.e., Sangiran, Zhoukoudian, and Dmanisi), while Ngandong is excluded in node H (see Figures 5 and 6). However, these trees fail to clarify the phylogenetic relationships between "Koobi fora – *H. habilis* s.l.", "Koobi fora – *H. ergaster*", the clade formed by Zhoukoudian, Dmanisi and Sangiran and Ngandong. In contrast, the trees obtained from matrix C, places all *H. erectus* sensu lato OTUs together at node F (see Figures 7 and 8), with "Koobi fora – *H. ergaster*" at node G, followed by Dmanisi at node H; at node I, Sangiran, Zhoukoudian, and Ngandong group together, with Zhoukoudian and Ngandong forming a monophyletic group at node J.

In these trees, the hypothetical ancestor of Ngandong, Neanderthals, and *H. sapiens* shares several morphological features. For example, in *norma lateralis*, the angle between the *planum occipital* and *planum nucale* is more pronounced compared to specimens from Dmanisi, Sangiran, and Zhoukoudian. Additionally, in *norma occipitalis*, the *processus retromastoideus* is absent, and the cranial outline is circular, or 'bomb-like,' as described in Neanderthals (Boule 1913, 1912, 1911; Condemi 1992; Vandermeersch 1981).

On the other hand, later studies proposed to group *H. ergaster* (African specimens) and *H. erectus* sensu stricto (Giava and China) into a single species, arguing that the differences between African and Asian populations are not enough to warrant separate species designations (Bräuer and Mbua 1992; Harrison 1993; Kennedy 1991; Kramer 1993). Some phylogenetic interpretations of the Dmanisi hominids in Georgia further support the idea of *H. erectus* as a single,

highly dimorphic species with significant temporal and geographic variation (Lordkipanidze et al. 2013; Vekua et al. 2002). On the other hand, genetic studies have suggested that the Ngandong specimens may belong to the Denisovan lineage or may be close to *H. sapiens* (Condemi and Savatier 2024; Ji et al. 2021; Ni et al. 2021; Shao et al. 2021; Zeitoun 2000). Interestingly, in the trees obtained from matrix C (see Figures 7 and 8), Dmanisi is included within *H. erectus* s.l. and supported by two synapomorphies (the outline of the supraorbital region in *norma facialis* is straight, and the *sulcus supraorbitalis* in the supraorbital region is incomplete), and the "Koobi Fora – *H. ergaster*" group is positioned just beneath it, supported by five characters (e.g., the position of the temporal squama is high and the outline of its superior border is rectilinear). Meanwhile, "Koobi Fora – *H. habilis* s.l." is placed at the root of the clade, emphasizing the bridge between Asian specimens (including the Ngandong specimens) and African specimens ("Koobi fora – *H. ergaster*"). Nevertheless, the results appear to support the existence of *H. erectus* s.s., which may be restricted to Eurasia during the Early and Middle Pleistocene, thus excluding specimens from Africa and Ngandong.

The analysis of the three matrices, each representing different data types, underscores the ongoing debate about the classification of *H. erectus* s.s. and *H. ergaster* and their position in the genus *Homo* (e.g., Antón 2003, 2002; Cameron et al. 2004; Dembo et al. 2016, 2015; Irish and Grabowski 2021; Martinón-Torres et al. 2007; Stringer 1987; Zeitoun 2000; Zeitoun et al. 2010). When analysing the PC scores, the resulting morphological characteristics of *H. ergaster* may resemble those of Ngandong and "Koobi fora – *H. habilis* s.l." more closely than *H. erectus* s.s.. This similarity makes it more difficult to clearly differentiate between those taxa. In contrast, the morphological approach treats the presence of multiple states as distinct, allowing for the inclusion of the different states in various scenarios before selecting the most parsimonious tree. In this context, it seems more reasonable to consider these two OTUs as more closely related taxa, especially when considering the shared set of characteristics used to distinguish them from other clades in two of the matrices.

The phylogenetic status and position of *H. neanderthalensis* has long been a subject of debate. Palaeogenomic data, suggesting admixture with *H. sapiens* populations (Fu et al. 2015; Green et al. 2010; Li et al. 2024; Prüfer et al. 2021) as well as the possibility of an isolated Neanderthal lineage in Europe (Slimak et al. 2024), have revived the debate over their taxonomic classification. In the present study, the OTUs "Early Neanderthals", "Near East Neanderthal" and "Classic Neanderthals" were created following the genetic study of Fabre et al. (2009). According to the results, the trees obtained from matrix A places the "Classic Neanderthals" at node K, the "Near East Neanderthals" at node L, and the "Early Neanderthals" at node M (see Figures 3 and 4). Similarly, the RC-weighted tree obtained from matrix B also supports the paraphyly of *H. neanderthalensis*. In this tree, the "Classic Neanderthals" are placed at node I, the "Early Neanderthals" at node J, and the "Near East Neanderthals" at node K. However, in the CI-weighted tree obtained from matrix B, the "Near East Neanderthal" and "Early Neanderthal" appear in a monophyletic group (node K, Fig. 5), as the sister group of *H. sapiens* (node L, Fig. 5), while the "Classic Neanderthal" are placed at the base of the clade (node J, Fig. 5).

Some authors (e.g., Ahern et al. 2002; Curnoe and Thorne 2003; Relethford 2001; Smith and Trinkaus 1991; Trinkaus 1991). Neanderthals and *H. sapiens* as variants of the same species, with the inclusion of the specimens from the Ngandong series (Bonde 1989; Bräuer and Mbua 1992; Campbell 1963; Dubois 1940; Gingerich 1979; Jelinek 1981, 1980; Stringer 1987; Tobias 1985; Von Koenigswald 1958; Widianto and Zeitoun 2003; Wolpoff 1980; Zeitoun et al. 2010). On the other hand, recent cladistic studies based on discrete morphological features (Mounier and Caparros 2015), as well as genetic evidence (Hajdinjak et al. 2018; Harvati et al. 2004; Hublin 2000; Ni et al. 2021; Rak 1993; White et al. 2014) support the existence

of two separate palaeontological species, which were nonetheless connected via geneflow from Africa to Europe during the second half of the Middle Pleistocene (Mounier and Mirazón Lahr 2019; Petr et al. 2020; Posth et al. 2017).

While the trees obtained from matrices A and B align with the hypothesis of a single, highly dimorphic species exhibiting significant temporal and geographic variation, the trees obtained from matrix C, based on 59 morphological features, groups all three OTUs into a monophyletic clade at node L, with bootstrap support of 72% for CI-weighting and 51% for RC-weighting (see Figures 7 and 8). In these trees, both the "Classic Neanderthals" and the "Near East Neanderthals" exhibit two autapomorphies, indicating a higher degree of differentiation compared to the "Early Neanderthals", (see Supplementary Material 14). This observation is consistent with the migration patterns of this group (Condemi 2007; Ghasidian et al. 2023; Profico et al. 2023; Voisin 2006), and the idea of several "Out-of-Africa" events during the late Middle Pleistocene (Mounier and Mirazón Lahr 2019; Petr et al. 2020; Posth et al. 2017) thus precluding the definition of boundaries of variability in early *H. sapiens* and the interpretation of individual fossils. Here we use a phylogenetic modelling method to predict possible morphologies of a last common ancestor of all modern humans, which we compare to LMP African fossils (KNM-ES 11693, Florisbad, Irhoud 1, Omo II, and LH18, which contributed to the evolution of the Neanderthals.

Regarding the *H. sapiens* populations, we decided to split the specimens into separate OTUs based on geographical groupings to test the coherence of the analyses at a sub-specific level. Interestingly, while the "Skhūl-Qafzeh" OTU appears as the root for *H. sapiens* in the trees based on morphological characters (node M, Figs. 7 and 8), it is placed inside the *H. sapiens* clade in the analysis of matrix A and B (node M, see Figures 3 to 6). Despite these ambiguities, all three trees consistently show *H. sapiens* as a monophyletic group, highlighting the value of this analytical approach.

For the taxa for which molecular data are available, the topologies recovered here are broadly consistent with genomic phylogenies (e.g., Meyer et al. 2016; Prüfer et al. 2014; Stringer 2016) particularly regarding the close relationships among *H. sapiens*, *H. neanderthalensis*, and other Late Pleistocene lineages. Minor incongruences are expected, however, as our analyses incorporate fossil OTUs for which no molecular data exist, and the inclusion of such taxa is known to affect tree reconstruction by introducing additional homoplastic or uncertain character information. Nonetheless, the overall agreement with genomic frameworks supports the biological plausibility of the results.

The length of the trees and the values of these indices vary depending on the weighting scheme used—showing fewer steps and higher indices for the RC weighting. The variation between the CI and RC weightings can be attributed to the fact that when a character exhibits homoplasy and the maximum homoplasy content for that character is important, adding additional homoplasy has a smaller effect on reducing the retention index (Goloboff 2022b). The effect of homoplasy on the retention index is moderated by the maximum possible homoplasy for a character, which depends on the number of taxa and the number of states that character can have. With characters with high potential for homoplasy, introducing more independent homoplastic changes has a reduced effect on lowering the retention index. As a result, the rescaled consistency index, which is the product of the consistency and retention indices, is less impacted (Goloboff 2022b).

The number of SPR moves and Robinson-Foulds (RF) distances varied according to the matrix used. Matrix A showed greater incongruence, while Matrix B produced more consistent topologies, particularly in the CI-weighted analysis, which demonstrated the highest level of congruence. The low congruence observed in Matrix A could be interpreted as supporting the argument that landmark data are not well-suited for phylogenetic reconstruction (Klingenberg and Gidaszewski 2010). However, an alternative explanation lies in the presence of polytomies in the trees generated

from Matrix B. Since both SPR and RF measures focus on conflicting nodes, they do not account for polytomies (Goloboff 2007), which may influence the apparent level of congruence in contrast with matrix A trees, who doesn't present any polytomies.

Overall, the results indicate that the phylogenetic trees are robust, with high consistency and retention indices. Considering both the morphological changes and the results, the trees obtained from matrices A and C appear to be the strongest trees. The trees obtained from matrix B, while showing strong indices, and lower SPR moves and RF distances, presents a large polytomy at their core (node E, Figures 5 and 6) and another polytomy in *H. sapiens* with the CI-weighting (node L, Fig. 5), undermining the robustness of the proposed phylogeny.

Although the difference is subtle, the results suggest that aligned landmark coordinates (matrix A) may yield slightly more reliable phylogenetic reconstructions than PC scores (matrix B), as indicated by marginally higher CI and RI values. Aligned coordinates preserve the spatial configuration of morphological traits, which can be advantageous when attempting to capture biologically meaningful variation—especially features traditionally emphasized in comparative morphology and discrete character analyses (Catalano et al. 2010; Goloboff 2022b; Monteiro 2000; Zelditch et al. 2004). That said, PC scores also have their strengths: by reducing dimensionality, they become mathematically independent. The observed differences in tree topologies are modest, and the presence of polytomies in some trees further complicates direct comparisons, particularly for SPR moves and RF distances. Ultimately, both approaches contribute valuable perspectives, and their combined use may offer a more comprehensive understanding of morphological evolution than either alone.

Finally, the results from the semi-calvarium were not significantly different from those derived from the whole calvarium (see Supplementary Material 9.3). Although the number of steps was slightly lower and the indices higher, the SPR values and RF distances were generally greater, indicating less congruent topologies.

Although the results obtained here are broadly coherent across datasets and weighting schemes, their robustness is inevitably constrained by several factors. These include small fossil sample sizes, the potential introduction of averaging artefacts during reconstruction and landmarking, and the presence of unresolved polytomies, all of which limit the confidence with which specific branching patterns can be interpreted. The sensitivity of the phylogenetic outcomes to data treatment—particularly in relation to semi-landmark placement, sliding procedures, and the use of different weighting schemes—further underscores the need for caution. As such, the topologies recovered should be considered provisional hypotheses whose stability must be re-evaluated through expanded sampling, increased anatomical coverage, and comparisons with independent lines of evidence. Future work would especially benefit from systematic assessments of alternative sliding strategies, including analyses conducted without sliding, as well as from exploring additional character-weighting approaches and the use of cost matrices to model variation in evolutionary change more explicitly.

Conclusions

In this study, we applied a standardized cladistic protocol to three distinct matrices, each representing a different type of data (landmark coordinates, principal component (PC) coordinates, and discrete morphological features). Despite differences between the resulting phylogenies, the overall patterns remain consistent, highlighting the value of incorporating 3D datasets into cladistic analyses. The results contribute to ongoing debates in palaeoanthropology, such as the taxonomical attribution of the specimens KNM-ER 1470 and 1813, the taxonomical status of specimens usually referred as *H. erectus* sensu lato and the phylogenetic relationships between *H. neanderthalensis* and *H. sapiens*. The present study only analyses the morphology of the calvarium and the obtained results must be interpreted cautiously, as cladistic analyses can be influenced by various

factors, such as character selection, OTU composition, and weighting methods (Arnold 1981; Chamberlain and Wood 1987). Indeed, the analysis of three different matrices related to the calvarium, each representing a distinct data type and following the same protocol, leads to varying yet coherent results that reflect different perspectives in the current discussion. The results and their contribution to current paleoanthropological discussions highlight the potential and reliability of this methodology, demonstrating that landmarks effectively capture morphologies that are usually described using morphological comparative methods, and that the resultant 3D data can be used in cladistics and can lead to improved phylogenetic resolution. Although the methodological and sampling limitations outlined above necessarily temper the strength of some inferences, they also help clarify the conditions under which morphometric phylogenetics performs most reliably. Despite these limitations, the present study demonstrates the considerable potential of integrating 3D geometric morphometric data into cladistic analyses. The congruence observed across different datasets—landmarks, PCs, and discrete characters—highlights the capacity of morphometric information to capture phylogenetically meaningful signal and to complement traditional morphological approaches. The methodological framework applied here provides a foundation for future, more extensive analyses that incorporate larger samples, more complete anatomical regions, and refined treatments of semi-landmarks, sliding procedures, and character weighting. By building on these strengths, subsequent research can further enhance the reliability of morphometric phylogenetics and contribute to increasingly robust reconstructions of hominin evolutionary history.

Acknowledgements

For permission to study specimens in their care, we thank directors and curators of the following institutions: Duckworth Laboratory, Cambridge; Ditsong National Museum of Natural History, Pretoria; Institut de Paléontologie Humaine, Paris; Musée de l'Homme, Paris; Museo di Antropologia "G. Sergi", Sapienza University of Rome; Museo delle Civiltà, Rome; National Museums of Kenya, Nairobi; ORSA database, Penn Museum; Peabody Museum, Cambridge; Senkenberg Forschungsinstiut und Naturmuseum, Frankfurt, and American Museum of Natural History, New York.
We also would like to thank Santiago Catalano, for his valuable help for scripting the protocols on TNT. The program TNT is freely available, thanks to a subsidy from the Willi Hennig Society.

Funding

This work was supported by Sapienza University of Rome (Ph.D. scholarship in Environmental and Evolutionary Biology - 38th cycle).

Data Availability Statement

The original data supporting the findings of this study are openly available in the supplementary materials.

Declaration of Interest

The authors declare no competing interests.

References

Abdi H and Williams L J (2010) Principal component analysis. Wiley Interdiscip Rev Comput Stat 2: 433–59. https://doi.org/10.1002/wics.101

Adams D C, Cardini A, Monteiro L R, et al (2011) Morphometrics and phylogenetics: Principal components of shape from cranial modules are neither appropriate nor effective cladistic characters. J Hum Evol 60: 240–3. https://doi.org/10.1016/j.jhevol.2010.02.003

Ahern J C M, Lee S-H, Hawks J D (2002) The late Neandertal supraorbital fossils from Vindija Cave, Croatia: a biased sample? J Hum Evol 43: 419–32. https://doi.org/10.1006/jhev.2002.0586

Andrews P (1984) An alternative interpretation of the characters used to define *Homo erectus*. Courier Forschungsinstitut Senckenberg 69: 167–75.

Antón S C (2002) Evolutionary significance of cranial variation in Asian *Homo erectus*. Am J Phys Anthropol 118: 301–23. https://doi.org/10.1002/ajpa.10091

Antón S C (2003) Natural history of *Homo erectus*. Am J Phys Anthropol 122: 126–70. https://doi.org/10.1002/ajpa.10399

Antón S C, Swisher C C (2004) Early dispersals of *Homo* from Africa. Annu Rev Anthropol 33: 271–96. https://doi.org/10.1146/annurev.anthro.33.070203.144024

Arnold E N (1981) Estimating phylogenies at low taxonomic levels. J Zool Syst Evol Res 19: 1–35.

Barriel V (1994) Les relations de parenté au sein des Hominoidea et la place de *Pan paniscus* : comparaison et analyse méthodologique des phylogénies morphologique et moléculaire, These de doctorat.

Blackwell B, Montoya A C, Bisson M S, et al (2007) ESR dating bovid teeth from Neanderthal layer at La Ferrassie, France. Geol Soc Am Bull 39: 548.

Blomberg S P, Garland JR. T, Ives A R (2003) Testing for phylogenetic signal in comparative data: behavioral traits are more labile. Evolution 57: 717–45. https://doi.org/10.1111/j.0014-3820.2003.tb00285.x

Bonde N (1989) *Erectus* and *neanderthalensis* as species or subspecies of *Homo* with a model of speciation in hominids. In: 2nd International Congress of Human Paleontology (ed) Hominidae, Jaca Book, Milan, p. 205–8.

Bookstein F L (1991) Morphometric tools for landmark data: geometry and biology, Cambridge University Press, Cambridge, p. 456.

Bookstein F L (1994) Can biometrical shape be a homologous character? In: Hall Brian K (ed) Homology: the hierarchial basis of comparative biology, Academic Press, San Diego, CA, pp 197–227

Bookstein F L (1997) Landmark methods for forms without landmarks: morphometrics of group differences in outline shape. Medical Image Analysis 1: 225–43. https://doi.org/10.1016/S1361-8415(97)85012-8

Bookstein F L (2002) Creases as morphometric characters. In: MacLeod N and Forey PL (eds) Morphology, Shape and Phylogeny, Taylor & Francis, London, p. 139–74.

Boule M (1911) L'homme fossile de La Chapelle-aux-Saints. Annales de Paléontologie 6.

Boule M (1912) L'homme fossile de La Chapelle-aux-Saints. Annales de Paléontologie 7: 105–92

Boule M (1913) L'homme fossile de La Chapelle-aux-Saints. Annales de Paléontologie 8: 1–62

Bräuer G, Mbua E 1992 *Homo erectus* features used in cladistics and their variability in Asian and African hominids. J Hum Evol 22: 79–108. https://doi.org/10.1016/0047-2484(92)90032-5

Broca P (1868) Sur les crânes et ossements des Eyzies. BMSAP 30: 335–49. https://doi.org/10.3166/bmsap-2018-0027

Broom R, Robinson J T (1950) Man contemporaneous with the Sawartkrans ape-man. Am J Phys Anthropol 8: 151–6. https://doi.org/10.1038/164322a0

Cameron D, Patnaik R, Sahni A (2004) The phylogenetic significance of the Middle Pleistocene Narmada hominin cranium from central India. Int J Osteoarchaeol 14: 419–47. https://doi.org/10.1002/oa.725

Campbell B (1962) The Systematics of Man. Nature 194: 225–32. https://doi.org/10.1038/194225A0

Campbell B (1963) Quantitative taxonomy and human evolution. In: Washburn SL (ed) Classification and Human Evolution, Taylor & Francis Group, London, pp 50–75.

Cardini A (2016) Lost in the other half: improving accuracy in geometric morphometric analyses of one side of bilaterally symmetric structures. Syst Biol 65: 1096–106. https://doi.org/10.1093/sysbio/syw043

Catalano S A, Ercoli M D, Prevosti F J (2015) The more, the better: The use of multiple landmark configurations to solve the phylogenetic relationships in musteloids. Syst Biol

64: 294–306. https://doi.org/10.1093/sysbio/syu107
Catalano S A, Goloboff P A, Giannini N P (2010) Phylogenetic morphometrics (I): the use of landmark data in a phylogenetic framework. Cladistics 26: 539–49. https://doi.org/10.1111/j.1096-0031.2010.00302.x
Catalano S A, Torres A (2017) Phylogenetic inference based on landmark data in 41 empirical data sets. Zool Scr 46: 1–11. https://doi.org/10.1111/zsc.12186
Chamberlain A T, Wood B A (1987) Early hominid phylogeny. J Hum Evol 16: 119–33. https://doi.org/10.1016/0047-2484(87)90063-7
Chambers J M (1992) Linear models. Chapter 4. In: Hastie T J (ed) Statistical Models in S, Wadsworth & Brooks/Cole, University of Michigan, p. 96–138.
Condemi S (2007) Are the Neanderthals in the levant? In: Faerman LKH M, Kahana et Uri Zilberman T (eds) Faces from the Past. Diachronic patterns in the biology of human populations from the eastern southern, Archaeopress, Oxford, pp 28–35.
Condemi S (1992) Les Hommes fossiles de Saccopastore et leurs relations phylogénétiques, CNRS Editions, Paris.
Condemi S, Savatier F (2024) L'énigme Denisova: après Néandertal et Sapiens, la découverte d'une nouvelle humanité, Albin Michel, Paris.
Copes L (2012) Comparative and experimental investigations of cranial robusticity in Mid-Pleistocene Hominins, These de doctorat, Arizona State University.
Curnoe D, Thorne A (2003) Number of ancestral human species: a molecular perspective. Homo 53: 201–24. https://doi.org/10.1078/0018-442X-00051
Dembo M, Matzke N J, Mooers A Ø, et al (2015) Bayesian analysis of a morphological supermatrix sheds light on controversial fossil hominin relationships. Proc. R. Soc. B. 282: 20150943. https://doi.org/10.1098/rspb.2015.0943
Dembo M, Radovčić D, Garvin H M, et al (2016) The evolutionary relationships and age of *Homo naledi*: An assessment using dated Bayesian phylogenetic methods. J Hum Evol 97: 17–26. https://doi.org/10.1016/j.jhevol.2016.04.008
Dubois E (1940) The fossil human remains discovered in Java by Dr. G.H.R. von Koenigswald and attribuated by him to *Pithecanthropus erectus*, in reality remains of *Homo sapiens soloensis*. Nederlandse Akademie van Wetenschappen 43: 841–54.
Fabre V, Condemi S, Degioanni A (2009) Genetic evidence of geographical groups among Neanderthals. PLoS One 4: e5151. https://doi.org/10.1371/journal.pone.0005151
Farris J (1983) The logical basis of phylogenetic analysis. In: Platnick NI and Funk VA (eds) Advances in Cladistics, Columbia University Press, New-York, p. 7–36.
Farris J S (1969) A successive approximations approach to character weighting. Syst zool 18: 374–85. https://doi.org/10.2307/2412182
Farris J S (1989) The retention index and the rescaled consistency index. Cladistics 5: 417–9. https://doi.org/10.1111/j.1096-0031.1989.tb00573.x
Feibel C S, Brown F H, McDougall I (1989) Stratigraphic context of fossil hominids from the Omo group deposits: Northern Turkana Basin, Kenya and Ethiopia. Am J Phys Anthropol 78: 595–622. https://doi.org/10.1002/ajpa.1330780412
Felsenstein J (2004) Inferring Phylogenies. Sinauer Associates, Sunderland, MA, p. 580.
Felsenstein J (1985) Phylogenies and the comparative method. Am Nat 125: 1–15. https://doi.org/10.1086/284325
Fu Q, Hajdinjak M, Moldovan O T, et al (2015) An early modern human from Romania with a recent Neanderthal ancestor. Nature 524: 216–9. https://doi.org/10.1038/nature14558
Gabounia L, Vekua A, Lordkipanidze D (2000) The environmental contexts of early human occupation of Georgia (Transcaucasia). J Hum Evol 38: 785–802. https://doi.org/10.1006/jhev.1999.0383
Ghasidian E, Kafash A, Kehl M, et al (2023) Modelling Neanderthals' dispersal routes from Caucasus towards east. PLoS One 18: e0281978. https://doi.org/10.1371/journal.pone.0281978

Giannini N P (2014) Quantitative developmental data in a phylogenetic framework. J Exp Zool B Mol Dev Evol 322: 558–66. https://doi.org/10.1002/jez.b.22588

Gingerich P D (1979) The stratophenetic approach to phylogeny reconstruction in vertebrate paleontology. In: Cracraft J, Eldredge N (eds) Phylogenetic analysis and paleontology: Proceedings of a symposium entitled "Phylogenetic Models," Convened at the North American Paleontological Convention II, Lawrence, Kansas, August 8, 1977, Columbia University Press, p. 41–78.

Goloboff P A (1993) Estimating character weights during tree search. Cladistics 9: 83–91. https://doi.org/10.1111/j.1096-0031.1993.tb00209.x

Goloboff P A (2007) Calculating SPR distances between trees. Cladistics 24: 591–7. https://doi.org/10.1111/j.1096-0031.2007.00189.x

Goloboff P A (2014) Oblong, a program to analyse phylogenomic data sets with millions of characters, requiring negligible amounts of RAM. Cladistics 30: 273–81. https://doi.org/10.1111/cla.12056

Goloboff P A (2022a) From observations to optimal phylogenetic trees: phylogenetic analysis of morphological data: Volume 1, Taylor & Francis Group, Milton.

Goloboff P A (2022b) Refining phylogenetic analyses: phylogenetic analysis of morphological data: Volume 2, Taylor & Francis Group, Milton.

Goloboff P A, Catalano S A (2011) Phylogenetic morphometrics (II): algorithms for landmark optimization. Cladistics 27: 42–51. https://doi.org/10.1111/j.1096-0031.2010.00318.x

Goloboff P A, Farris J S, Nixon K C (2008) TNT, a free program for phylogenetic analysis. Cladistics 24: 774–86. https://doi.org/10.1111/j.1096-0031.2008.00217.x

Goloboff P A, Mattoni C I, Quinteros A S (2006) Continuous characters analyzed as such. Cladistics 22: 589–601. https://doi.org/10.1111/j.1096-0031.2006.00122.x

Goloboff P A, Morales M E (2023) TNT version 1.6, with a graphical interface for MacOS and Linux, including new routines in parallel. Cladistics 39: 144–53. https://doi.org/10.1111/cla.12524

González-José R, Escapa I, Neves W A, et al (2008) Cladistic analysis of continuous modularized traits provides phylogenetic signals in *Homo* evolution. Nature 453: 775–8. https://doi.org/10.1038/nature06891

Green R E, Krause J, Briggs A W, et al (2010) A draft sequence of the Neandertal genome. Science 328: 710–22. https://doi.org/10.1126/science.1188021

Grimaud D (1982) Evolution du pariétal de l'homme fossile. Position de l'Homme de Tautavel parmi les hominidés, Thèse de doctorat, Université de Provence, Aix-Marseille, p. 705.

Grün R, Stringer C B (1991) Electron spin resonance dating and the evolution of modern humans. Archaeometry 33: 153–99. https://doi.org/10.1111/j.1475-4754.1991.tb00696.x

Grün R, Stringer C, McDermott F, et al (2005) U-series and ESR analyses of bones and teeth relating to the human burials from Skhul. J Hum Evol 49: 316–34. https://doi.org/10.1016/j.jhevol.2005.04.006

Gunz P, Mitteroecker P (2013) Semilandmarks: a method for quantifying curves and surfaces. Hystrix 24. https://doi.org/10.4404/hystrix-24.1-6292

Gunz P, Mitteroecker P, Bookstein F L (2005) Semilandmarks in three dimensions. In: Slice DE (ed) Modern morphometrics in physical anthropology, Springer US, Boston, MA, p. 73–98. https://doi.org/10.1007/0-387-27614-9_3

Hajdinjak M, Fu Q, Hübner A, et al (2018) Reconstructing the genetic history of late Neanderthals. Nature 555: 652–6. https://doi.org/10.1038/nature26151

Harrison T (1993) Cladistic concepts and the species problem in hominoid evolution. In: Kimbel WH, Martin LB (eds) Species, Species Concepts and Primate Evolution, Springer US, Boston, MA, p. 345–71.

Harvati K, Frost S R, McNulty K P (2004) Neanderthal taxonomy reconsidered: Implications of 3D primate models of intra- and interspecific differences. Proc Natl

Acad Sci USA 101: 1147–52. https://doi.org/10.1073/pnas.0308085100

Hawkins J A, Hughes C E, Scotland R W (1997) Primary homology assessment, characters and character states. Cladistics 13: 275–83. https://doi.org/10.1111/j.1096-0031.1997.tb00320.x

Hublin J-J (2000) Modern-nonmodern hominid interactions: a mediterranean perspective. In: Bar-Yosef O, Pilbeam D (eds) The geography of Neandertals and modern humans in Europe and the greater Mediterranean, Harvard Peabody Museum, Cambridge, p. 157–82

Irish J D, Grabowski M (2021) Relative tooth size, Bayesian inference, and *Homo naledi*. Am J Phys Anthropol 176: 262–82. https://doi.org/10.1002/ajpa.24353

Jelinek J (1980) European *Homo erectus* and the origin of *Homo sapiens*. In: Current arguments on early man, Pergamon, Oxford, p. 137–44.

Jelinek J (1981) Was *Homo erectus* already *Homo sapiens*? In: Ferembach D (ed) Les processus de l'hominisation, CNRS Editions, p. 85–9.

Ji Q, Wu W, Ji Y, et al (2021) Late Middle Pleistocene Harbin cranium represents a new *Homo* species. Innovation 2: 100132. https://doi.org/10.1016/j.xinn.2021.100132

Jolliffe I T (2002) Principal component analysis for special types of data. In: Jolliffe I T (ed) Principal Component Analysis, Springer-Verlag, New York, p. 338–72.

Kendall D G (1977) The diffusion of shape. Adv Appl Probab 9: 428–30. https://doi.org/10.2307/1426091

Kennedy G E (1991) On the autapomorphic traits of *Homo erectus.* J Hum Evol 20: 375–412. https://doi.org/10.1016/0047-2484(91)90006-H

Klingenberg C P (2010) Evolution and development of shape: integrating quantitative approaches. Nat Rev Genet 11: 623–35. https://doi.org/10.1038/nrg2829

Klingenberg C P, Gidaszewski N A (2010) Testing and quantifying phylogenetic signals and homoplasy in morphometric data. Syst Biol 59: 245–61. https://doi.org/10.1093/sysbio/syp106

Klingenberg C P, Marugán-Lobón J (2013) Evolutionary covariation in geometric morphometric data: analyzing integration, modularity, and allometry in a phylogenetic context. Syst Biol 62: 591–610. https://doi.org/10.1093/sysbio/syt025

Klingenberg C P, McIntyre G S (1998) Geometric morphometrics of developmental instability: Analyzing patterns of fluctuating asymmetry with Procrustes methods. Evol 52: 1363–75. https://doi.org/10.1111/j.1558-5646.1998.tb02018.x

Klingenberg C P, Monteiro L R (2005) Distances and directions in multidimensional shape spaces: Implications for morphometric applications. Syst Biol 54: 678–88. https://doi.org/10.1080/10635150590947258

Kramer A (1993) Human taxonomic diversity in the pleistocene: Does *Homo erectus* represent multiple hominid species? Am J Phys Anthropol 91: 161–71. https://doi.org/10.1002/ajpa.1330910203

Larick R, Ciochon R L, Zaim Y, et al (2001) Early Pleistocene 40Ar/39Ar ages for Bapang Formation hominins, Central Jawa, Indonesia. Proc Natl Acad Sci USA 98: 4866–71. https://doi.org/10.1073/pnas.081077298

Li L, Comi T J, Bierman R F, Akey J M (2024) Recurrent gene flow between Neanderthals and modern humans over the past 200,000 years. Science 385: eadi1768. https://doi.org/10.1126/science.adi1768

Lockwood C A, Kimbel W H, Lynch J M (2004) Morphometrics and hominoid phylogeny: Support for a chimpanzee-human clade and differentiation among great ape subspecies. Proc Natl Acad Sci USA 101: 4356–60. https://doi.org/10.1073/pnas.0306235101

Lordkipanidze D, Ponce de León M S, Margvelashvili A, et al (2013) A complete skull from Dmanisi, Georgia, and the evolutionary biology of early *Homo.* Science 342: 326–31. https://doi.org/10.1126/science.1238484

MacLeod N, Forey P L (2002) Phylogenetic signals in morphometric data. In: MacLeod N and Forey P L (eds) Morphology, shape and phylogeny, Taylor & Francis, London, p. 100–38

Marra F, Ceruleo P, Jicha B, et al (2015) A new age within MIS 7 for the *Homo neanderthalensis* of Saccopastore in the glacio-eustatically forced sedimentary successions of the Aniene River Valley, Rome. Quat Sci Rev 129: 260–74. https://doi.org/10.1016/j.quascirev.2015.10.027

Martinón-Torres M, Castro J M B de, Gómez-Robles A, et al (2007) Dental evidence on the hominin dispersals during the Pleistocene. Proc Natl Acad Sci USA 104: 13279–82. https://doi.org/10.1073/pnas.0706152104

Matile L, Tassy P, Goujet D (1987) Introduction à la systématique zoologique (concepts, principes, méthodes), Société française de systématique, Paris, p. 126.

McCracken K G, Harshman J, McClellan D A et al (1999) Data set incongruence and correlated character evolution: an example of functional convergence in the hind-limbs of stifftail diving ducks. Syst Biol 48: 683–714. https://doi.org/10.1080/106351599259979

Meyer M, Arsuaga J-L, de Filippo C, et al (2016) Nuclear DNA sequences from the Middle Pleistocene Sima de los Huesos hominins. Nature 531: 504–7. https://doi.org/10.1038/nature17405

Monteiro L R (2000) Why morphometrics is special: The problem with using partial warps as characters for phylogenetic inference. Syst Biol 49: 796–800. https://www.jstor.org/stable/2585294

Mounier A (2009) Validité du taxon *Homo heidelbergensis* Schoetensack, 1908, These de doctorat, Aix-Marseille 2

Mounier A, Balzeau A, Caparros M, et al (2016) Brain, calvarium, cladistics: A new approach to an old question, who are modern humans and Neandertals? J Hum Evol 92: 22–36. https://doi.org/10.1016/j.jhevol.(2015.12.006

Mounier A, Caparros M (2015) The phylogenetic status of *Homo heidelbergensis* – a cladistic study of Middle Pleistocene hominins. BMSAP 27: 110–34. https://doi.org/10.1007/s13219-015-0127-4

Mounier A, Heuzé Y, Samsel M, et al (2020) Gravettian cranial morphology and human group affinities during the European Upper Palaeolithic. Sci Rep 10: 21931. https://doi.org/10.1038/s41598-020-78841-x

Mounier A, Marchal F, Condemi S (2009) Is *Homo heidelbergensis* a distinct species? New insight on the Mauer mandible. J Hum Evol 56: 219–46. https://doi.org/10.1016/j.jhevol.2008.12.006

Mounier A, Mirazón Lahr M (2016) Virtual ancestor reconstruction: Revealing the ancestor of modern humans and Neandertals. J Hum Evol 91: 57–72. https://doi.org/10.1016/j.jhevol.2015.11.002

Mounier A, Mirazón Lahr M (2019) Deciphering African late middle Pleistocene hominin diversity and the origin of our species. Nat Commun 10: 3406. https://doi.org/10.1038/s41467-019-11213-w

Mounier A, Villotte S, Kacki S, et al (2024) Population affinities in pre-colonial West Africa: The case of the burial cave Iroungou (Gabon, 14th–15th century CE). Am J Biol Anthropol 185: e24997. https://doi.org/10.1002/ajpa.24997

Nelson G (1978) Ontogeny, phylogeny, paleontology, and the biogenetic law. Syst Zool 27: 324-45. https://doi.org/10.2307/2412883

Ni X, Ji Q, Wu W, et al (2021) Massive cranium from Harbin in northeastern China establishes a new Middle Pleistocene human lineage. Innovation 2: 100130. https://doi.org/10.1016/j.xinn.2021.100130

Olivier G (1960) Pratique anthropologique, Vigot Frères, Paris, p. 299.

Pagel M (1999) Inferring the historical patterns of biological evolution. Nature 401: 877–84. https://doi.org/10.1038/44766

Palci A, Lee M S Y (2019) Geometric morphometrics, homology and cladistics: review and recommendations. Cladistics 35: 230–42. https://doi.org/10.1111/cla.12340

Parins-Fukuchi C (2018) Use of continuous traits can improve morphological phylogenetics. Syst Biol 67: 328–39. https://doi.org/10.1093/sysbio/syx072

Pélabon C, Firmat C, Bolstad G H, et al (2014) Evolution of morphological allometry. Ann N Y Acad Sci 1320: 58–75. https://doi.org/10.1111/nyas.12470

Perrard A, Lopez-Osorio F, Carpenter J M (2016) Phylogeny, landmark analysis and the use of wing venation to study the evolution of social wasps (*Hymenoptera: Vespidae: Vespinae*). Cladistics 32: 406–25. https://doi.org/10.1111/cla.12138

Petr M, Hajdinjak M, Fu Q, et al (2020) The evolutionary history of Neanderthal and Denisovan Y chromosomes. Science 369: 1653–6. https://doi.org/10.1126/science.abb6460

de Pinna M C C (1991) Concepts and tests of homology in the cladistic paradigm. Cladistics 7: 367–94. https://doi.org/10.1111/j.1096-0031.1991.tb00045.x

Pleijel F (1995) On character coding for phylogeny reconstruction. Cladistics 11: 309–15. https://doi.org/10.1016/0748-3007(95)90018-7

Pogue M G, Mickevich M F (1990) Character definitions and character state delineation: the bete noire of phylogenetic inference. Cladistics 6: 319–61. https://doi.org/10.1111/j.1096-0031.1990.tb00549.x

Posth C, Wißing C, Kitagawa K, et al (2017) Deeply divergent archaic mitochondrial genome provides lower time boundary for African gene flow into Neanderthals. Nat Commun 8: 16046. https://doi.org/10.1038/ncomms16046

Profico A, Buzi C, Di Vincenzo F, et al (2023) Virtual excavation and analysis of the early Neanderthal cranium from Altamura (Italy). Commun Biol 6: 1–8. https://doi.org/10.1038/s42003-023-04644-1

Prüfer K, Posth C, Yu H, et al (2021) A genome sequence from a modern human skull over 45,000 years old from Zlatý kůň in Czechia. Nat Ecol Evol 5: 820–5. https://doi.org/10.1038/s41559-021-01443-x

Prüfer K, Racimo F, Patterson N, et al (2014) The complete genome sequence of a Neanderthal from the Altai Mountains. Nature 505: 43–9. https://doi.org/10.1038/nature12886

Rak Y (1993) Morphological variation in *Homo neanderthalensis* and *Homo sapiens* in the Levant. In: Kimbel WH, Martin LB (eds) Species, species concepts and primate evolution: advances in primatology, Springer US, Boston, MA, pp 523–36. https://doi.org/10.1007/978-1-4899-3745-2_20

Relethford J H (2001) Absence of regional affinities of Neandertal DNA with living humans does not reject multiregional evolution. Am J Phys Anthropol 115: 95–8. https://doi.org/10.1002/ajpa.1060

Rink W J, Schwarcz H p., Lee H K, et al (2001) Electron spin resonance (ESR) and thermal ionization mass spectrometric (TIMS) 230Th/234U dating of teeth in Middle Paleolithic layers at Amud Cave, Israel. Geoarchaeology 16: 701–17. https://doi.org/10.1002/gea.1017

Rizal Y, Westaway K E, Zaim Y, et al (2020) Last appearance of *Homo erectus* at Ngandong, Java, 117,000–108,000 years ago. Nature 577: 381–5. https://doi.org/10.1038/s41586-019-1863-2

Robinson D F, Foulds L R (1981) Comparison of phylogenetic trees. Math Biosci 53: 131–47. https://doi.org/10.1016/0025-5564(81)90043-2

Rohlf F J (2001) Comparative methods for the analysis of continuous variables: geometric interpretations. Evolution 55: 2143–60. https://doi.org/10.1111/j.0014-3820.2001.tb00731.x

Rohlf F J (2002) Geometric morphometrics and phylogeny. In MacLeod N, Forey PL (eds) Morphology, Shape and Phylogeny, Taylor & Francis, London, p. 175–93.

Rohlf F J (1998) On applications of geometric morphometrics to studies of ontogeny and phylogeny. Syst Biol 47: 147–58. https://www.jstor.org/stable/2585239

Rohlf F J, Bookstein F L (1987) A comment on shearing as a method for "size correction". Syst Zool 36: 359–68. https://doi.org/10.2307/2413400

Schwarcz H P, Grün R, Tobias P V (1994) ESR dating studies of the australopithecine site of Sterkfontein, South Africa. J Hum Evol 26: 175–81. https://doi.org/10.1006/jhev.1994.1010

Sereno P C (2007) Logical basis for morphological characters in phylogenetics. Cladistics 23: 565–87. https://doi.org/10.1111/j.1096-0031.2007.00161.x

Shao Q, Ge J, Ji Q, et al (2021) Geochemical provenancing and direct dating of the Harbin archaic human cranium. Innovation 2. https://doi.org/10.1016/j.xinn.2021.100131

Shen G, Gao X, Gao B, et al (2009) Age of Zhoukoudian *Homo erectus* determined with 26Al/10Be burial dating. Nature 458: 198–200. https://doi.org/10.1038/nature07741

Simon-Maciejewski M, Manzi G, Zeitoun V, et al (2024) Cladistics with geometric morphometric data: The variability of the calvarium in the genus *Homo*. BMSAP 36. https://doi.org/10.4000/bmsap.14053

Slimak L, Vimala T, Seguin-Orlando A, et al (2024) Long genetic and social isolation in Neanderthals before their extinction. Cell Genom 4. https://doi.org/10.1016/j.xgen.2024.100593

Smith F H, Trinkaus E (1991) Les origines de l'homme moderne en Europe centrale : un cas de continuité. In Hublin J-J and Tillier AM (eds) Aux origines d'*Homo sapiens*, Press Universitaires de France, Paris, p. 251–90.

Smith U E, Hendricks J R (2013) Geometric morphometric character suites as phylogenetic data: Extracting phylogenetic signal from gastropod shells. Syst Biol 62: 366–85. https://doi.org/10.1093/sysbio/syt002

Stringer C B (1987) A numerical cladistic analysis for the genus *Homo*. J Hum Evol 16: 135–46. https://doi.org/10.1016/0047-2484(87)90064-9

Stringer C B (2016) The origin and evolution of *Homo sapiens*. Philos Trans R Soc Lond B Biol Sci 371: 20150237. https://doi.org/10.1098/rstb.2015.0237

Swofford D, Olsen G J, Waddell P J, et al (1996) Phylogenetic Inference. In: Hillis DM, Moritz C and Mable B K (eds) Molecular Systematics, 2nd Edition, Sinauer Associates, Sunderland, MA, p. 407–514.

Tattersall I (1986) Species recognition in human paleontology. J Hum Evol 15: 165–75. https://doi.org/10.1016/S0047-2484(86)80043-4

Thiele K (1993) The Holy grail of the perfect character: The cladistic treatment of morphometric data. Cladistics 9: 275–304. https://doi.org/10.1111/j.1096-0031.1993.tb00226.x

Tobias P V (1985) Single characters and total morphological pattern redefined the sorting effected by a selection of morphological features of the early hominids. In: Delson E (ed) Ancestors: The Hard Evidence, A.R. Liss, Michigan, p. 94–101.

Trinkaus E (1991) Les Hommes fossiles de la grotte de Shanidar, Irak : évolution et continuité parmi les Hommes archaïques et tardifs du Proche-Orient. Anthropologie 95: 535–72.

Vandermeersch B (1981) Les Hommes de Qafzeh (Israël), Paris.

Varón-González C, Whelan S, Klingenberg C P (2020) Estimating phylogenies from shape and similar multidimensional data: Why it is not reliable. Syst Biol 69: 863–83. https://doi.org/10.1093/sysbio/syaa003

Vekua A, Lordkipanidze D, Rightmire G P, et al (2002) A new skull of early *Homo* from Dmanisi, Georgia. Science 297: 85–9. https://doi.org/10.1126/science.1072953

Voisin J L (2006) Speciation by distance and temporal overlap: a new approach to understanding Neanderthal evolution. In: Hublin J-J, Harvati K and Harrison T (eds.) Neanderthals Revisited: New Approaches and Perspectives, Springer Netherlands, Dordrecht, p. 299–314. https://doi.org/10.1007/978-1-4020-5121-0_17.

Von Koenigswald G H R (1958) Der Solo-Mensch von Java: ein tropischer Neanderthaler. Hundert Jahre Neanderthaler: 21–6.

Wheeler W (2001) Homology and the optimization of DNA sequence data. Cladistics 17: S3–11. https://doi.org/10.1006/clad.2000.0154

Wheeler W C (2021) Distance Wagner tree refinement as a heuristic approach to character-based initial tree construction. Cladistics 37: 829–37. https://doi.org/10.1111/cla.12478

White S, Gowlett J A J, Grove M (2014) The place of the Neanderthals in hominin phylogeny. J Anthropol Archaeol 35: 32–50. https://doi.org/10.1016/j.jaa.2014.04.004

Widianto H, Zeitoun V (2003) Morphological description, biometry and phylogenetic position of the skull of Ngawi 1 (east Java, Indonesia). Int J Osteoarchaeol 13: 339–51. https://doi.org/10.1002/oa.694

Wiley D F (2005) Landmark. Institute for Data Analysis and Visualization, University of California, Davis

Wolpoff M H (1980) Cranial remains of Middle Pleistocene European hominids. J Hum Evol 9: 339–58. https://doi.org/10.1016/0047-2484(80)90047-0

Wood B A (1984) The origin of *Homo erectus.* Courrier Forschungsinstitut Senckenberg 69: 99–111

Zeitoun V (2003) High occurrence of a basicranial feature in *Homo erectus*: Anatomical description of the preglenoid tubercle. Anat Rec B New Anat 274B: 148–56. https://doi.org/10.1002/ar.b.10028

Zeitoun V (2000) Révision de l'espèce *Homo erectus* (Dubois, 1893). BMSAP 12: 1–200. https://doi.org/10.4000/bmsap.5963

Zeitoun V, Détroit F, Grimaud-Hervé D, Widianto H (2010) Solo man in question: Convergent views to split Indonesian *Homo erectus* in two categories. Quat Int 223–224: 281–92. https://doi.org/10.1016/j.quaint.2010.01.018

Zelditch M L, Swiderski D L, Sheets H D (2004) Geometric morphometrics for biologists. A primer, Elsevier/Academic Press, Amsterdam.

Editor, Giovanni Destro Bisol

***Appendix** - Description of each morphological feature and character state. Percentage of missing data for each character is indicated; for more details see **Mounier and Caparros (2015)** and **Mounier et al. (2016)**.*

MORPHOLOGICAL FEATURES	% MISSING DATA	CHARACTER STATES	
1) Outline of the calvarium, *norma occipitalis*	0	1	triangular
		2	circular
		3	pentagonal
2) Frontal cord length / parietal cord length	2,56	1	Frontal < Parietal
		2	Frontal ≈ Parietal
		3	Frontal > Parietal
3) Outline of the supraorbital region, *norma facialis*	2,56	1	straight
		2	convex
4) Supraorbital region: *sulcus supraorbitalis*	2,56	1	complete
		2	incomplete
		3	absent: *arcus superciliaris* and *supraorbitalis* merged
5) Projection of the supraorbital region	0	1	not projecting
		2	*arcus superciliaris* only
		3	whole supraorbital region
6) Post-orbital constriction (Ipc=M9/M43)	0	1	important (Ipc<0.75)
		2	weak (0.75≥Ipc≥0.85)
		3	absent (Ipc>0.85)
7) Outline of the supraorbital region, *norma verticalis*	2,56	1	medially concave (glabella)
		2	straight
		3	convex
8) *Sulcus postorbitalis*	1,28	1	absent
		2	medially present
		3	present continue
9) *Tuber frontale*	0	1	absent
		2	defined, medially shifted
		3	present
10) Antero-posterior convexity of the frontal (Ifc=M29*100/M26)	2,56	1	weak (Ifc>95)
		2	intermediate (95>Ifc≥90)
		3	important (Ifc<90)
11) *Linea temporalis* development on the frontal	0	1	absent
		2	present, unique
		3	present, double
12) Sagittal keel on the frontal	0	1	absent
		2	present
13) Bregmatic eminence	0	1	absent
		2	present
14) Pterion (antero-lateral region of the skull formed by the junction of the frontal, the parietal, the sphenoid and the temporal)	0	1	spheno-parietal
		2	fronto-temporal
15) Thickening on the superior part of the coronal sutures	0	1	absent
		2	present
16) Sagittal keel on the bregma-lambda arch	1,28	1	absent
		2	present

Appendix* - *Continued.

MORPHOLOGICAL FEATURES	% MISSING DATA	CHARACTER STATES	
17) Parasagittal hollowing on both sides of the parietal suture	0	1	absent
		2	present
18) Pre-lambdatic hollowing on the bregma-lambda arch	0	1	absent
		2	present
19) *Linea temporalis* width of the temporal band	0	1	absent
		2	narrow (<20mm)
		3	wide (≥20mm)
20) *Linea temporalis*: position on parietal (Rlt = temporo-parietal suture-superior line / temporo-parietal suture-bregma)	0	1	high (Rlt>0.55)
		2	medial (0.54>Rlt>0.46)
		3	low (Rlt<0.45)
21) *Torus angularis parietalis*	0	1	absent
		2	present
22) *Tuber parietale*	0	1	absent
		2	present, medially shifted
		3	present, high position
23) Outline of the occipital, *norma lateralis*	0	1	rounded profile
		2	sharply angled
24) Outline of the *planum occipitale*, *norma lateralis*	0	1	no convexity
		2	convexity
25) Relative development: *planum nucale* (PN) / *planum occipitale* (PO)	2,56	1	PN≥PO
		2	PN<PO
26) Occipital bun	0	1	absent
		2	present
27) Opisthocranion relative position / inion	0	1	same position
		2	different position
28) *Processus retromastoideus*	2,56	1	absent
		2	present
29) Outline of the *planum occipitale*, *norma occipitalis*	1,28	1	triangular
		2	circular
		3	pentagonal
30) Suprainiac fossa	0	1	absent
		2	hollowing, weakly-delineated
		3	present
31) Suprainiac fossa: lateral edges	0	1	absent
		2	convergent upward
		3	parallels or arched
32) *Sulcus supratoralis*	0	1	absent
		2	hollowing
		3	present
33) *Torus occipitalis transversus*	0	1	absent
		2	present: medially protruding
		3	present: bilaterally protruding

Appendix* - *Continued.

MORPHOLOGICAL FEATURES	% MISSING DATA	CHARACTER STATES
34) *Torus occipitalis transversus* form, *norma occipitalis*	0	1 absent 2 rectilinear 3 convex
35) *Protuberantia occipitalis externa*	1,28	1 absent 2 present
36) *Tuberculum linearum*	1,28	1 absent 2 present
37) External occipital crest	5,13	1 absent 2 present, posterior only 3 present
38) Aligned posterior and anterior external occipital crest	7,7	1 yes 2 no
39) Temporal squama heigh (Iet=maximal height from *auriculae100 / maximal width)**	0	1 low (Iet ≤ 60) 2 high (Iet> 60)
40) Outline of the anterior border of the temporal squama	2,56	1 curved or sinuous 2 rectilinear
41) Outline of the superior border of the temporal squama	0	1 curved or sinuous 2 rectilinear
42) Development of the *crista supramastoidea* at the porion	0	1 absent 2 weakly marked 3 marked
43) *Crista supramastoidea* / *processus zygomaticus temporalis*	2,56	1 not lined up 2 lined up
44) *Tuberculum supramastoideum anterius*	0	1 absent 2 present
45) Supramastoid groove (between *crista supramastoidea* and *crista mastoidea*)	1,28	1 absent 2 present, closed anteriorly 3 present
46) Form of the auditory meatus	1,28	1 circular 2 elliptic
47) Position of the auditory meatus / *processus zygomaticus temporalis*	2,56	1 below 2 intermediate 3 lined up
48) *Tuberculum mastoideum anterior*	1,28	1 absent 2 present
49) *Processus mastoideus*: downward development / basicranium	6,4	1 weak 2 strong
50) Juxtamastoid ridge development / *processus mastoideus*	8,97	1 less developed 2 as developed 3 more developed
51) Digastric groove: presence of a bony bridge	3,85	1 no 2 yes

***Appendix** - Continued.*

MORPHOLOGICAL FEATURES	% MISSING DATA	CHARACTER STATES	
52) ***Crista occipito mastoidea***	10,25	1	absent
		2	present
53) Glenoid cavity depth / articular tubercle lowest point	0	1	shallow (<0.9 mm)
		2	deep (>0.9 mm)
54) Petro-tympanic crest orientation in relation to the sagittal plan	0	1	perpendicular
		2	frontward
		3	backward
55) Articular tubercle configuration	0	1	medio-lateral concavity
		2	antero-posterior convexity
		3	medio-lateral convexity and vertical
56) ***Tuberculum zygomaticum anterius***	3,85	1	absent to weakly marked
		2	marked
57) ***Tuberculum zygomaticum posterius*** **(post glenoid process)**	2,56	1	absent to weakly marked
		2	marked
58) Tympanal contribution to the posterior wall of the glenoid cavity	1,28	1	weak
		2	important
59) Preglenoid tubercle	1,28	1	absent
		2	present